UNIVERSIDADE FEDERAL DO PARANÁ

YOHAN SZUSZKO SOARES

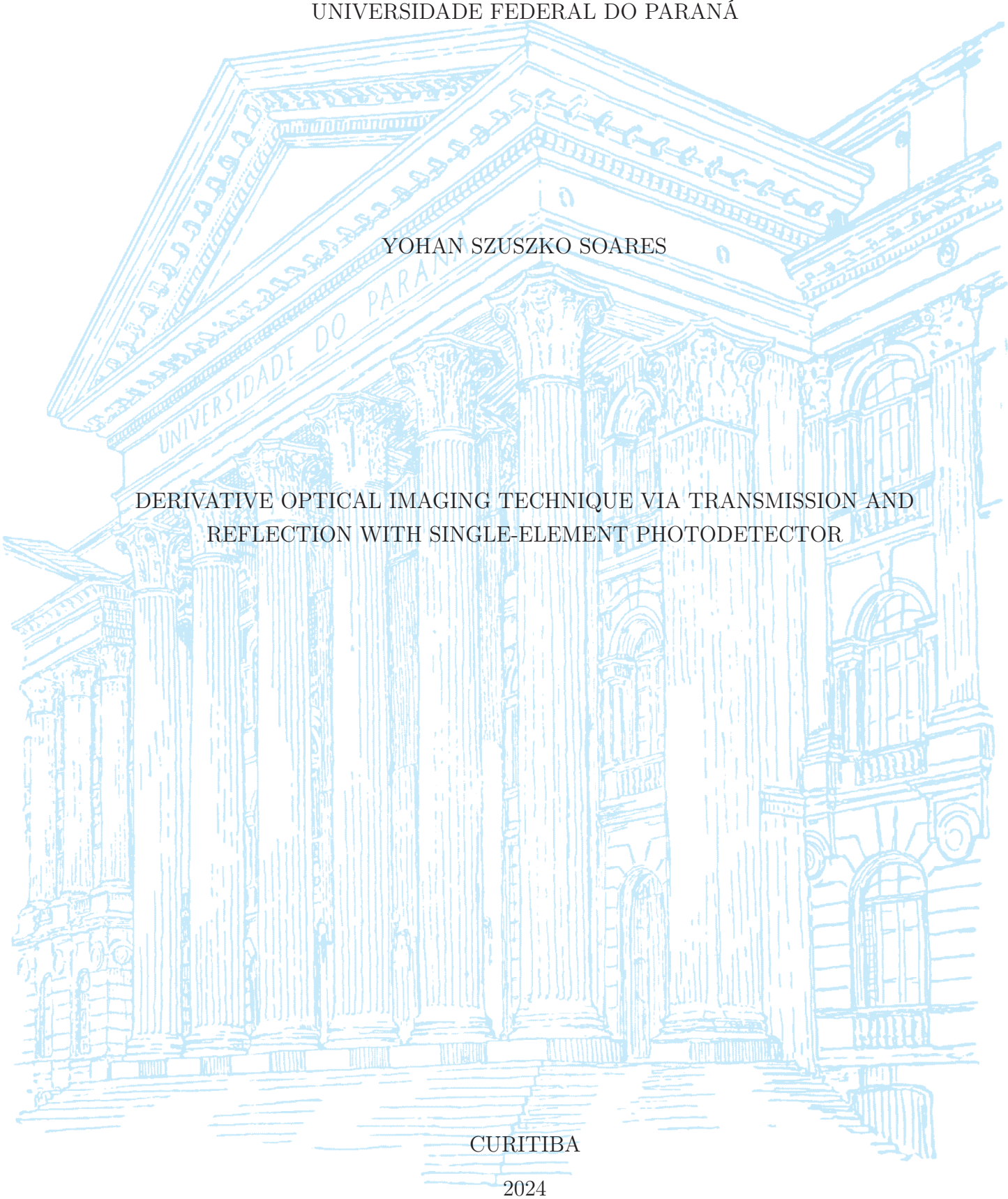

DERIVATIVE OPTICAL IMAGING TECHNIQUE VIA TRANSMISSION AND REFLECTION WITH SINGLE-ELEMENT PHOTODETECTOR

CURITIBA

2024

YOHAN SZUSZKO SOARES

DERIVATIVE OPTICAL IMAGING TECHNIQUE VIA TRANSMISSION AND REFLECTION WITH SINGLE-ELEMENT PHOTODETECTOR

Dissertação apresentada ao Programa de Pós-Graduação em Física do Setor de Ciências Exatas da Universidade Federal do Paraná como requisito parcial para a obtenção de título de Mestre em Física.

Supervisor: Prof. Dr. Emerson Cristiano Barbano

CURITIBA

2024

DADOS INTERNACIONAIS DE CATALOGAÇÃO NA PUBLICAÇÃO (CIP)
UNIVERSIDADE FEDERAL DO PARANÁ
SISTEMA DE BIBLIOTECAS – BIBLIOTECA DE CIÊNCIA E TECNOLOGIA

Soares, Yohan Szuszko
Derivative optical imaging technique via transmission and reflection with single-element photodetector / Yohan Szuszko Soares. – Curitiba, 2024.
1 recurso on-line : PDF.

Dissertação (Mestrado) - Universidade Federal do Paraná, Setor de Ciências Exatas, Programa de Pós-Graduação em Física.

Orientador: Emerson Cristiano Barbano

1. Imagens ópticas. 2. Microscopia. 3. Detectores ópticos. 4. Imageamento de Pixel Único. I. Universidade Federal do Paraná. II. Programa de Pós-Graduação em Física. III. Barbano, Emerson Cristiano. IV. Título.

Bibliotecário: Elias Barbosa da Silva CRB-9/1894

APPROVAL MINUTE

The Examining Board is designated by the Faculty of the Graduate Program of the Federal University of Paraná in FÍSICA where invited to argue the THESIS of MASTER OF SCIENCES by **YOHAN SZUSZKO SOARES** , entitled: **"Derivative optical imaging technique via transmission and reflection with single-element photodetector"**, under the supervision of Dr. EMERSON CRISTIANO BARBANO, which and after assessment of the candidate and the work, the Examining Board decided for the Approval in the present rite.

The granting of the title of master of sciences is contingent upon the fulfillment of all the requirements indicated by the Examining Board and terms determined in the regulation of the Graduate Program.

CURITIBA, August 01th, 2024.

EMERSON CRISTIANO BARBANO
President of the Examining Board

TSUNEYUKI OZAKI
External Member (INSTITUT NATIONAL DE LA RECHERCHE SCIENTIFIQUE)

RANDY BARTELS
External Member (MORGRIDGE INSTITUTE FOR RESEARCH)

CAMILLA KARLA BRITES QUEIROZ MARTINS DE OLIVEIRA
Internal Member(UNIVERSIDADE FEDERAL DO PARANÁ)



OPTICA








MAFIA
DO
CAPTER


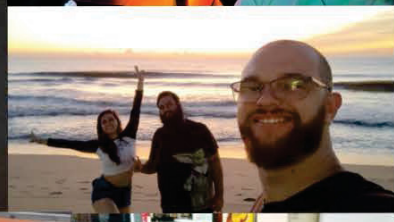






DEPARTAMENTO DE
FÍSICA

imaginação

RESUMO

Microscópios desempenham um papel fundamental nas ciências, especialmente na saúde e na ciência dos materiais. O desenvolvimento e aprimoramento dos sistemas de microscopia impactam diretamente essas áreas, justificando o esforço contínuo para criar instrumentos melhores. Com o advento dos lasers, tornou-se mais fácil utilizar processos ópticos não lineares que permitem a obtenção de imagens com maior resolução. Técnicas como SPIFI (Spatial Frequency-modulated Imaging) ganharam reconhecimento por sua configuração simples, aquisição rápida, compatibilidade com meios dispersores e capacidade de obter imagens de alta resolução. Este método de imagem é baseado na detecção de uma linha focal de um feixe de laser focado por uma lente cilíndrica, usando um detector de elemento único. Cada ponto dessa linha é modulado por uma máscara rotativa, correspondendo a uma frequência temporal única. Ao realizar uma integração temporal do sinal coletado pelo detector e aplicar uma Transformada de Fourier, esse sinal pode ser transformado em um mapeamento espacial das localizações únicas ao longo da linha geométrica. Em busca de novas técnicas, propomos o Derivative Optical Imaging Technique (DOIT), baseada no SPIFI. O DOIT usa um fotodetector de elemento único e um chopper óptico para modular o feixe, com características espaciais codificadas temporalmente. O sinal do objeto, capturado pelo detector de elemento único, é analisado por meio de derivadas temporais para revelar sua organização espacial. Neste trabalho, desenvolvemos o DOIT para coletar sinais por meio de transmissão. Além disso, criamos uma variação chamada Re-DOIT (Reflective DOIT), que coleta informações refletidas pela amostra. Apresentamos os princípios de funcionamento desses microscópios, bem como resultados que indicam a viabilidade dessas técnicas e possíveis aplicações.

Palavras-chaves: Imageamento Óptico. Microscopia. Imageamento de Pixel Único.

ABSTRACT

Microscopes play a fundamental role in the sciences, particularly in healthcare and materials science. The development and enhancement of microscopy systems directly impact these fields, justifying the continuous effort to create better instruments. With the advent of lasers, it has become easier to utilize nonlinear optical processes that enable higher-resolution images. Techniques such as SPIFI (SPatIal Frequency-modulated Imaging) have gained recognition for their simple setup, fast acquisition, compatibility with scattering media, and ability to obtain high-resolution images. This imaging method is based on the detection of a focal line from a laser beam focused by a cylindrical lens, using a single-element detector. Each point on this line is modulated by a rotating mask, corresponding to a unique temporal frequency. By performing a temporal integration of the signal collected by the detector and applying a Fourier Transform, this signal can be transformed into a spatial mapping of the unique spatial locations along the geometric line. In search of new techniques, we propose the Derivative Optical Imaging Technique (DOIT), based on SPIFI. DOIT uses a single photodetector and an optical chopper to modulate signals, with spatial characteristics temporally encoded. The object's signal, captured by the single-element detector, is analyzed through temporal derivatives to reveal its spatial organization. In this work, we developed DOIT to collect signals through transmission. Additionally, we created a variation called ReDOIT (Reflective DOIT), which collects information reflected by the sample. We present the operating principles of these microscopes as well as results that indicate the feasibility of these techniques and possible applications.

Key-words: Optical Imaging. Microscopy. Single-Pixel Imaging.

List of Figures

Contents

— 1 —

The Beginning

1.1 NEW CHAPTER OF AN OLD STORY

In the field of optical imaging, advancements have been made to improve resolution and image contrast over time. One key factor in enhancing resolution is the use of shorter wavelengths (λ), as demonstrated by the relationship formalized by Ernst Abbe in the equation $d_{Abbe} = \lambda/2NA$ [1, 2, 3]. This equation highlights the minimum size of a resolvable self-luminous point and the optic's capacity to resolve it, with a particular focus on the numerical aperture (NA) parameter. By utilizing shorter wavelengths, microscopists have been able to enhance resolution.

Optical imaging is indispensable in scientific research and diverse practical applications, offering insights into complex samples and systems [4, 5]. Achieving high-resolution imaging and capturing details are fundamental requirements, and emerging single-beam methods such as Spatial Frequency-modulated Imaging (SPIFI) [6, 7, 8, 9] are at the forefront of enabling these capabilities by providing faster scanning imaging with a single-element photodetector and compatibility with scattering media. However, developing new techniques, such as the one proposed by this work, Derivative Optical Imaging Technique (DOIT), remains essential for advancing the field and addressing evolving challenges.

These methodologies enable us to extract intricate details from optical systems, transcending traditional limitations and deepening our comprehension of complex phenomena. By enhancing optical imaging, these approaches contribute to significant discoveries and applications across various scientific domains, broadening our horizons of knowledge and exploratory possibilities.

In optical imaging, there exists a persistent challenge when venturing into the infrared spectrum: the absence of suitable cameras for image capture [10, 11, 12]. This limitation restricts researchers from fully exploring the potential of infrared imaging, hindering progress in fields such as astronomy, environmental monitoring, and biomedical imaging. Recognizing this barrier, our research endeavors to address this gap by intro-

ducing a new technique called DOIT. By leveraging single-element photodetectors, DOIT works around the dependency on CCD cameras, offering a novel approach to imaging in infrared ranges where traditional imaging devices fall short.

This project introduces the Derivative Optical Imaging Technique, representing a departure from the traditional SPIFI methodology [13]. While SPIFI relies on the Fast Fourier Transform (FFT) for signal analysis, DOIT leverages derivatives to capture nuanced optical imaging details. In DOIT, we conduct imaging via transmission, which is particularly useful for objects with low light absorption. Additionally, we have explored an alternative setup resulting in a novel approach called Reflective DOIT (ReDOIT), which essentially applies the principles of DOIT to reflection imaging. ReDOIT proves to be valuable for analyzing the surfaces of objects, offering a versatile approach for optical characterization.

Chapter 2 delves into the Single Pixel Technique, SPIFI as documented in the article published in the Brazilian Journal of Physics Education (RBEF), alongside the description of the novel DOIT and ReDOIT techniques. Additionally, Chapter 2 conducts a comprehensive literature review, scoping the fundamentals of optical imaging and delving into detailed explanations of the SPIFI, DOIT, and ReDOIT techniques, along with their mathematical underpinnings and practical applications. The chapter discusses the limitations and challenges inherent in the SPIFI technique, which served as the impetus for the development of DOIT, focusing particularly on modulation challenges, and ReDOIT, addressing surface analysis concerns. Furthermore, previous research on optical imaging and spatial frequency modulation techniques is reviewed to provide a contextual backdrop for the study.

In Chapter 3, the methodology employed in the study is elucidated, detailing the experimental procedures undertaken to develop and evaluate the SPIFI, DOIT, and ReDOIT techniques. Implementation specifics for each technique are outlined, along with the comparison methodologies utilized to contrast DOIT and ReDOIT with SPIFI.

Chapter 4 showcases the results obtained from the application of the SPIFI, DOIT, and ReDOIT techniques. A thorough comparison of the results across these methodologies is conducted, accompanied by a comprehensive discussion on the relative advantages and limitations of each technique variant.

The ensuing Chapter 5 embarks on a nuanced discussion, interpreting the obtained results, particularly focusing on resolution aspects at both ordinary and high orders. The implications of the findings for the broader field of optical imaging are examined, along with reflections on the potential applications of the DOIT/ReDOIT techniques in various contexts, including their compatibility with alternative light sources.

In Chapter 6, the conclusion chapter, the key findings and discoveries of the

study are recapitulated. Final conclusions are drawn regarding the efficacy and feasibility of DOIT and ReDOIT techniques *vis-à-vis* SPIFI. Furthermore, suggestions for future research avenues and developmental trajectories within the realm of optical imaging are put forth, aiming to propel the field forward.

— 2 —

A Pragmatic Guide to Single-Pixel Imaging

2.1 INTRODUCTION: LOOKING WITH A SINGLE EYE

Optical imaging, encompassing a broad range of techniques utilizing light for visualizing and analyzing objects, has become indispensable across various scientific and technological domains. From medical diagnostics to materials science, optical imaging plays a fundamental role in providing valuable insights into the structure, composition, and behavior of diverse materials and biological specimens.

Single-Pixel Imaging (SPI) has emerged as a groundbreaking technique for image acquisition in various scientific and technological domains. Single-Pixel Imaging microscopy techniques date back to the 1960s [14], and now various linear and nonlinear optical processes are commonly employed to produce 2D images in optically transparent media. This approach, fundamentally different from conventional imaging techniques, offers a novel perspective to address challenges associated with capturing images in adverse conditions, low light environments, and beyond the visible spectrum.

In the domain of non-visible wavelength single-pixel imaging, the short-wave infrared (SWIR) spectral region (approximately 1-3 μm) has accumulated significant attention due to the availability of highly sensitive detectors [15, 16]. Specifically, advancements in telecommunications research have yielded a variety of InGaAs devices [17], facilitating the development of both cost-effective detectors and illumination sources operating within the 800 nm to 1800 nm range. This spectral range has demonstrated efficacy in imaging through scattering media, such as smoke [18], and has also proven useful in detecting and imaging hydrocarbon gas leaks [19].

The continuous advancement of optical imaging technologies reflects the ongoing efforts of researchers to enhance imaging instruments and methodologies. For instance, in the realm of medical imaging, optical coherence tomography (OCT) has emerged as a powerful tool for non-invasive visualization of biological tissues with high resolution and depth penetration [5]. In materials science, optical imaging techniques are essential for characterizing the properties and behavior of materials at various length scales. Recent

developments, such as spatially modulated laser beam imaging methods proposed by [6, 7, 8], demonstrate innovative approaches to enhance spatial resolution and sensitivity in material imaging.

The basic principle behind SPI involves reconstructing a two-dimensional image of a scene using only a single-element detector and an efficient scanning process. In most techniques that employ a laser beam, laser scanning or sample scanning is implemented to collect information capable of obtaining an image [20, 21]. This is achieved through the modulation of incident light and the application of advanced image reconstruction algorithms. SPI is intriguing because it circumvents the need for traditional cameras to form images, relying instead on single-element detectors, which are more cost-effective and available in a wide range of spectral bands.

During the data acquisition process in SPI, the scene of interest is illuminated with specific light patterns, such as scattering, polarization changes, harmonic generation, or fluorescence excitation light, which are modulated and directed towards a single-element detector. This detector measures the light interacting with the scene at different points in time or position, resulting in a temporal series of measurements. Subsequently, reconstruction algorithms are applied to decode the information contained in this temporal series and reconstruct the two-dimensional image of the scene.

The applications of SPI are vast and span across various fields of knowledge. In medicine, for instance, this technique has the potential to revolutionize image acquisition in endoscopic procedures, cancer detection, and intraoperative imaging, enabling high-resolution images in low-light conditions. In security and defense sectors, SPI can be employed in night vision, aerial surveillance, and target detection under adverse conditions. In astronomy, it enables the acquisition of high-resolution images of astronomical objects in regions of the electromagnetic spectrum where conventional telescopes face limitations.

With the development of the laser [22], laser scanning microscopy producing a point-by-point image is widely used in research. Due to the significantly long time to form a complete image, researchers have sought to develop alternative techniques with multi-beam systems [4]-[23]. However, these are more complicated techniques to implement and less financially viable. An alternative is to use a focal line instead of a focal point, which can be obtained by focusing the beam with a cylindrical lens.

A cylindrical lens, unlike a spherical lens, consists of a transparent material capable of causing all rays of light from an incident parallel beam to pass very close to a single line as they emerge from the other side of the lens, forming a focal line. This occurs because the cylindrical lens collimates the laser beam in a single direction, without affecting the beam in the direction perpendicular to it due to the special curvature of the lens (Figure 1). This focal line follows the Gaussian intensity distribution profile ($u(x)$), where the center is more intense than the edges. Figure 1 compares the laser beam before

and after passing through a cylindrical lens and shows the power distribution along the radial coordinate of each beam.

Figure 1 – Gaussian laser beam before and after passing through the cylindrical lens. When passing through the cylindrical lens, at its focus, the beam is compressed in one direction forming a focal line.

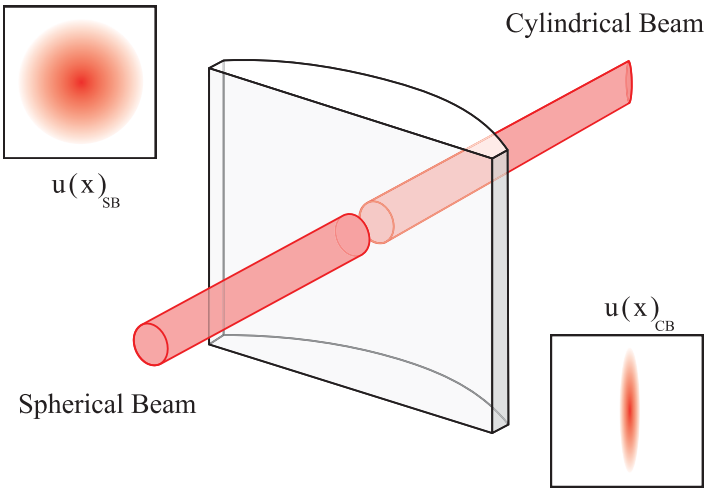

Source: Adapted from [9].

2.2 SPATIAL FREQUENCY-MODULATED IMAGING TECHNIQUE - SPIFI

This chapter introduces an illumination technique suitable for extended geometries utilizing a single-element detector. The illumination is encoded by a mask with a carrier frequency modulation pattern, which varies according to position. Either the mask or the illumination can be moved relative to each other. Although the mask can assume various geometries, the outcome remains consistent: the spatial frequencies of the mask are translated into temporal (carrier) frequencies on the illumination.

2.2.1 Introduction

In 2011, Futia et al [13] introduced a new method of fluorescent luminescent imaging with a single-element photodetector. Multiple-acquisition photodetectors, such as CCDs (Charge-coupled device), have the disadvantage that photons incident on the sample may scatter and follow a non-ballistic path to the CCD, so they may be recorded at an "incorrect" position on the 2D photodetector, thereby decreasing the image quality. This phenomenon is known as scattering ambiguity (Figure 2).

The solution to avoid the scattering using the focal line was to modulate at different frequencies the distinct parts of the line, that is, to encode in frequency the small parts of the beam along the length of the focal line [24]. Another advantage of this system, in which the excitation beam is modulated (multiplexed) in spatial frequency, is that light can be collected by a single-element photodetector.

Figure 2 – Scattering scheme. We have a focal line incident on a sample, and as it interacts with the sample, the light scatters. Parts of the beam that reach different parts of the CCD will be in distinct positions, resulting in a loss of resolution.

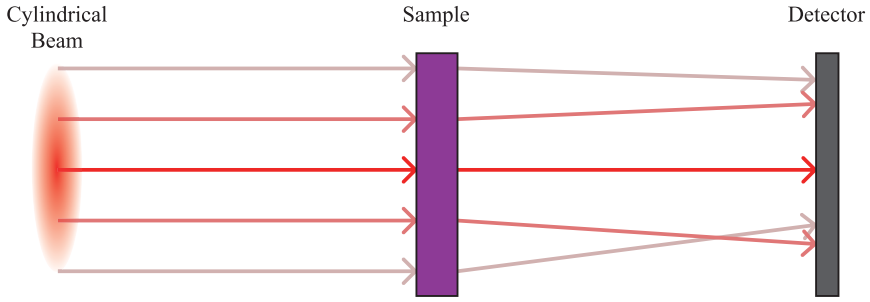

Source: Adapted from [9].

This technique [13, 25, 26, 27], encodes the spatial information of different parts of the focal line at certain frequencies, through the use of a rotating mask [24]. Thus, the intensity modulation of the beam incident on the sample should be transmitted to the light collected at the photodetector, regardless of the optical process that produced this light during the interaction of radiation with matter.

2.2.2 Modulated Imaging

Frequency modulation in SPIFI is a key technique that encodes spatial information into the frequency components of the excitation beam. This modulation is achieved through the use of a spinning modulation disk, Lovell's reticle [28] (Figure 3), which introduces a specific modulation pattern to the excitation light beam. The modulation mask will modulate the intensity, in amplitude, with a spatial frequency that increases linearly along the extension of the focal line. In other words, Figure 3 shows us that points close to the center of the mask (red line) will have a lower frequency compared to points further away from the center of the disk (green line).

Figure 3 – Modulation mask used for the SPIFI technique. Different parts of the beam are at distinct frequencies. In red, we have a lower frequency, and as we move away from the center of the mask, the modulation frequency increases (in purple and green).

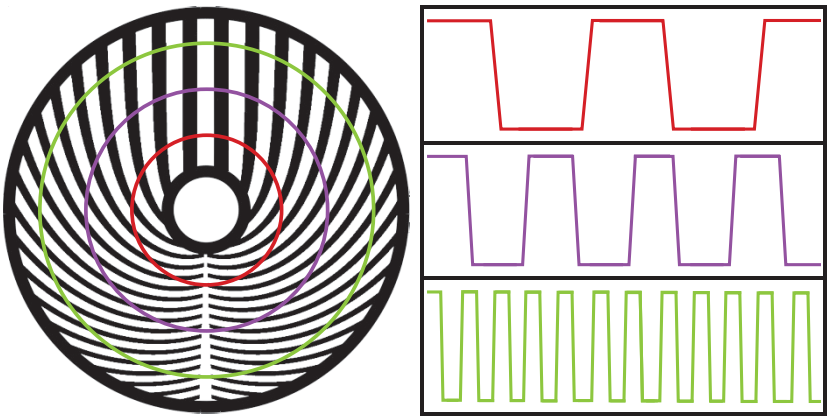

Source: Adapted from [9].

The modulation pattern, typically represented as $m(x,t)$, is applied to the excitation beam, affecting the object field by modulating it with the object's transmission function $g(x)$. The object field, denoted as $E_{obj}(x,t)$, can be expressed as:

$$E_{obj}(x,t) = E_0 u(x) m(x,t) g(x) e^{(i\omega_0 t)}, \tag{2.1}$$

where ω_0 is the frequency of the excitation light, E_0 is the amplitude of the electric field, and $u(x)$ is the normalized spatial field of the beam (a line cursor with a Gaussian shape).

By modulating the excitation beam with a specific pattern and analyzing the resulting signal detected by a photodiode, SPIFI can recover spatial information from a time-only signal. This modulation technique allows for the extraction of spatial details from the frequency components of the detected signal, enabling high-resolution spatial imaging without the blurring effects of scattering crosstalk.

In the context of SPIFI, a single-element detector measures the intensity of the electric field rather than the electric field itself. The intensity of light reaching the photodetector can be expressed as:

$$I_{obj}(x,t) = I_0 \mid u(x) m(x,t) g(x) \mid^2, \tag{2.2}$$

where $I_0 = \frac{cn\epsilon_0}{2}|E_0|^2$, where c is the speed of light in vacuum, ϵ_0 the electric permittivity of vacuum, n the refractive index of the medium, and I_0 is the intensity of the laser. We can obtain an expression for the signal recorded by the detector:

$$s(t) = \gamma \int I(x,t) dx, \tag{2.3}$$

where γ includes factors such as detector and system optical efficiency.

The modulation used by [13], represented in equation 2.4, can be rewritten in the coordinate system of the electric field as follows:

$$m(x,t) = \frac{w(t)}{2}[1 + cos(2\pi\kappa x t)], \tag{2.4}$$

where $w(t)$ represents the finite time-window of the modulator.

By focusing the modulated signal with a spherical lens onto a sample, we induce spatial and temporal interference between the different parts of the modulated beam. This interference effect occurs because, at the focus of the spherical lens, there will be a spatial and temporal overlap of electric fields with different oscillation frequencies (according to the modulation of the mask). This overlap of fields at different frequencies gives rise to a pulse, which is the characteristic signal of the SPIFI technique.

2.2.3 Imaging System

In this imaging technique, optical components are used to expand and collimate the light beam before it reaches the cylindrical lens (which will provide us with the focal line). The modulation, as described in Section 2.2.2, will modulate the intensity, in amplitude (the intensity reaching the single-element detector varies over time), with a frequency that increases linearly along the extension of the focal line (Figure 3). In Figure 4, we can visualize the assembly of the imaging technique in a summarized manner.

Figure 4 – Experimental setup of the SPIFI technique, adapted from [13]. In red, we have the laser beam, which passes through the cylindrical lens (CL) generating a focal line and a Spherical Lens (SL) to focus onto the mask and collimate the beam. The beam then passes through the mask and is focused by the objective lens (OL) onto the sample. Finally, the beam is focused by the Collection Optics (CO) on the detector for signal collection.

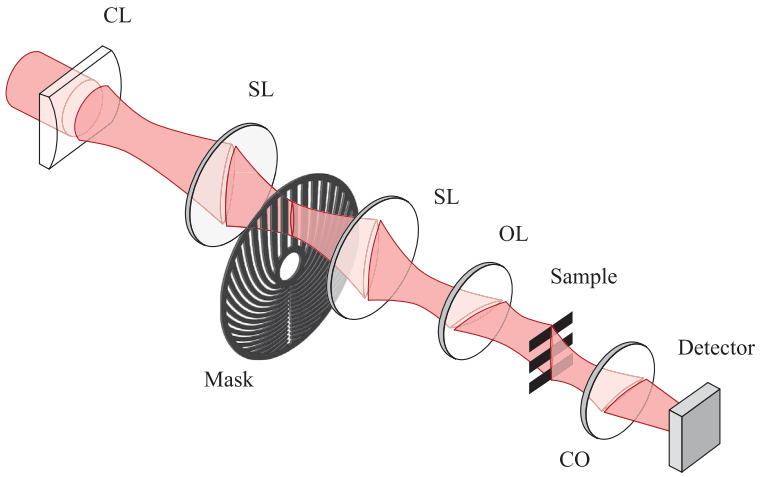

Source: Adapted from [13].

The beam is then modulated by the rotating mask in both the temporal and spatial domains. As it passes through the modulation mask, the beam is focused onto the sample by the lens OL. This interaction can be modeled in terms of the electric field and by a function that varies in the spatial domain, as described in Section 2.2.2. In this technique, we can employ linear and nonlinear optical processes to obtain an image in order to increase resolution or obtain complementary information. Working with fluorescence microscopy [13], for example, this process can represent the concentration of fluorophores, which are molecules that absorb photons with energy from a specific excitation spectrum and re-emit them with energy in a specific emission (or fluorescence) spectrum.

2.2.4 SPIFI Signal

When a sample is positioned at the focus of the spherical lens (OL), part of the cylindrical beam is blocked by the sample. This induces spatial and temporal interference among different sections of the modulated beam (Figure 5). The spherical lens focus causes

an overlap of electric fields with varying oscillation frequencies, as dictated by the mask modulation. This overlapping of fields at different frequencies produces a pulse, depicted in Figure 6, which is the defining signal of the SPIFI technique.

Figure 5 – Sample partially blocking the cylindrical beam. Using a objective lens to focus the line on the needle, part of the signal is blocked by the sample, and the collected signal will differ from the signal without the presence of a sample.

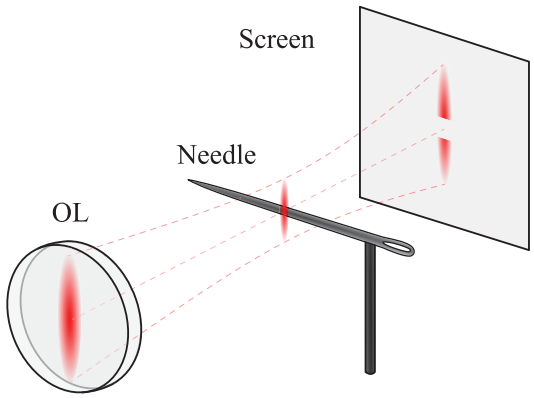

Source: Adapted from [9].

Figure 6 – SPIFI Signal without sample (black) and with a sample (red). Due to the presence of the sample, part of the beam is blocked, and the collected signal will not contain the same range of frequencies as the original signal. This reduction in frequency content represents the spatial distribution of the sample.

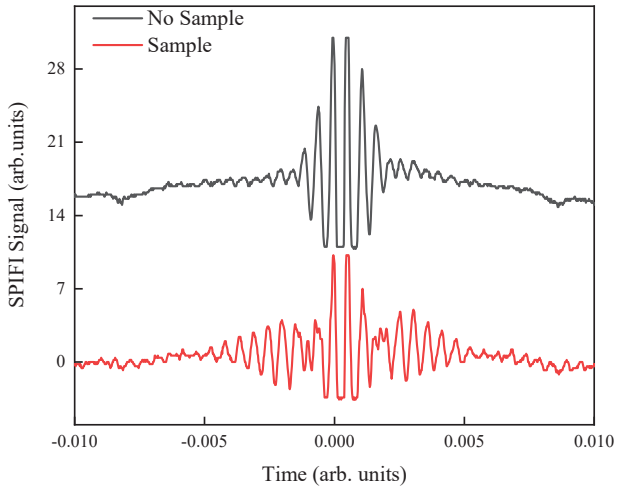

Source: The Author.

To form a one-dimensional image, in addition to collecting the signal from the focal line along the entire sample, we must process the signal $s(t)$, signal collected by the photodetector, by applying a Fourier Transform to convert the signal into a frequency mapping, corresponding to the unique spatial locations of each point along the geometrical line. The Fourier Transform converts this temporal signal into the corresponding

modulation frequency, which reflects the Gaussian profile of the laser, as shown in Figure 7. This transform represents a line of the magnified image.

Figure 7 – Fast Fourier Transform of the first order SPIFI Signal without sample (black) and with a sample (red). It can be observed that the FFT of the black signal represents a Gaussian profile modulated at different spatial frequencies. The red signal represents the same profile, but with missing frequencies, indicating the sample blocking the beam.

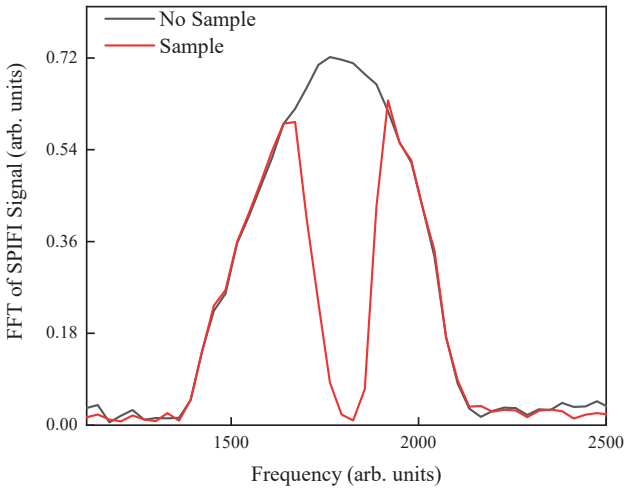

Source: The Author.

When applying the Fast Fourier Transform (FFT) to a signal, the different orders of the FFT represent integer multiples of the signal's fundamental frequency. For instance, in the first order of the FFT, we have the fundamental frequencies associated with the signal with 600 different units of frequencies for that spatial region (Figure 7). In the second-order (Figure 8), these frequencies are doubled, resulting in 1200 units of frequencies for the same spatial region, and so forth for subsequent orders. This means that the higher orders of the FFT provide increased resolution, as more frequencies are associated with the same spatial interval. In other words, the higher the order of the FFT, the more detailed the representation of spatial variations in the signal, allowing for a more accurate reconstruction of the spatial distribution of intensities.

Figure 8 – Fast Fourier Transform of high orders SPIFI Signal without sample (black) and with a sample (red). Note that the first and second order FFTs represent the same object information, but the second-order image has twice the frequencies, resolving the Gaussian profile better. This results in an increased resolution, meaning that more pixels can resolve the object.

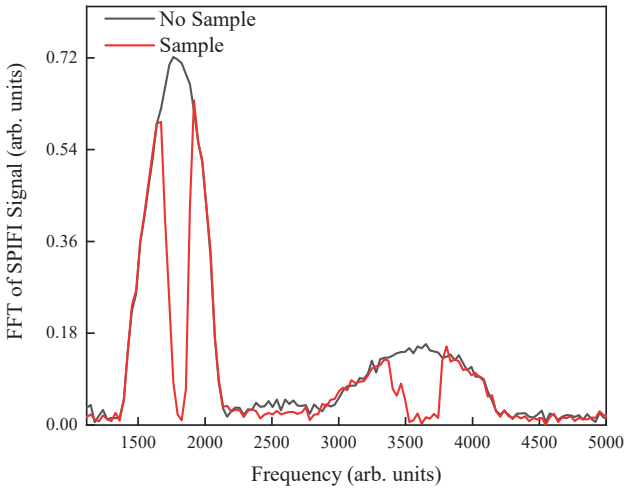

Source: The Author.

2.3 JUST DOIT. SOMETIMES REDOIT

This chapter introduces a new imaging technique suitable for extended geometries utilizing a single-element detector, based on the SPIFI principle. The illumination is encoded with a carrier frequency modulation, performed by an optical chopper. This approach allows obtaining images with a resolution similar to SPIFI, but is experimentally simpler due to how the cylindrical beam modulation is performed.

2.3.1 Introduction

Similar to how the FRITE [24] technique inspired SPIFI [13] development in 2011, we have followed a similar path to create a new single-pixel imaging technique. While SPIFI employs a modulation mask that encodes the cylindrical beam into different spatial and temporal frequencies, the Derivative Optical Imaging Technique, or just DOIT, utilizes only an optical chopper that encodes the focal line at a single frequency, based on the spatial modulation (in intensity) of the laser beam incident on the sample.

Unlike SPIFI, in the DOIT technique, the signal modulated by the optical chopper generates a smoothed periodic waveform, which can be described as an oscillatory Heaviside function with a fixed frequency. The analysis and conversion of the signal into spatial information are then performed by applying temporal differentiation to the signal, resulting in the spatial distribution of the modulated beam.

2.3.2 Modulated Imaging

Starting from Equation 2.1, representing the electric field, we can express our modulation by an oscillatory Heaviside function with length L and period $T/2$ (as it takes half a period for the signal to transition from completely blocked to completely unblocked, due to the rotation of the optical chopper blade). The Heaviside function:

$$H(x) = \frac{1}{2} + \frac{1}{2}\text{sgn}(x). \tag{2.5}$$

Therefore, we can write the modulation as:

$$m(x,t) = H\left[\sin\left(\frac{\pi x}{L} - \frac{2\pi t}{T}\right)\right]. \tag{2.6}$$

Note that due to the beam being Gaussian, this implies that the beam intensity is uniform across the entire region of interest. In this case, the variation of the modulated signal over time and space is mainly governed by the modulation function $m(x,t)$, which describes how the signal is modulated with respect to position x and time t. Therefore, we can rewrite Equation 2.3 as follows:

$$s(t) = \gamma \int_0^L m(x,t)dx = \gamma \int_0^L H\left[\sin\left(\frac{\pi x}{L} - \frac{2\pi t}{T}\right)\right] dx. \tag{2.7}$$

Developing equation 2.7, by applying the Heaviside function to the sine function, gives rise to the function $a(t)$, which determines where the sine function is positive or negative, and consequently where the Heaviside function evaluates to 1 or 0. This function serves as the lower limit of the spatial intensity integral, and as it varies over time, the result of the integral provides a function of time. Physically, $a(t)$ represents the position of the edge of the chopper blade, serving as the boundary between the blocked and unblocked signal regions. We can express $a(t)$ as:

$$a(t) = \begin{cases} \frac{2tL}{T}, & \text{if } 0 \leq t < \frac{T}{2}, \\ 0, & \text{if } \frac{T}{2} \leq t < T. \end{cases} \tag{2.8}$$

Now, considering the Gaussian profile of the laser:

$$I(x,t) = I_0 \mid m(x,t)u(x)g(x)e^{i\omega_0 t} \mid^2, \tag{2.9}$$

with no sample blocking the beam $g(x) = 1$ and the Gaussian beam is describe by $u(x) = e^{\frac{(x-L/2)^2}{w_0^2}}$, we have the signal $s(t)$:

$$s(t) = \gamma I_0 e^{i\omega_0 t} \int_0^L m^2(x,t)u^2(x)dx. \tag{2.10}$$

Mathematically manipulating equation 2.10, we should arrive at:

$$s(t) = \begin{cases} \sqrt{\frac{\pi}{8}}\gamma I_0 e^{i\omega_0 t} w_0 \left\{ \text{erf}\left[\frac{L}{\sqrt{2}w_0}\right] - \text{erf}\left[\frac{L(\frac{4t}{T}-1)}{\sqrt{2}w_0}\right]\right\}, & \text{if } 0 \leq t < \frac{T}{2}, \\ 0, & \text{if } \frac{T}{2} \leq t < T. \end{cases} \tag{2.11}$$

Now, the derivative signal is proportional to the derivative of the detected signal:

$$D_s(t) = \frac{d}{dt}s(t). \tag{2.12}$$

We will disregard the contribution of the oscillatory term of the electromagnetic field, as it is orders of magnitude higher and its oscillation cannot be detected. Finally, the derivative signal can be written as:

$$D_s(t) = -\frac{2L}{T}\gamma I_0 e^{i\omega_0 t} exp\left[-\frac{L^2\left(\frac{4t}{T}-1\right)^2}{2w^2}\right]. \tag{2.13}$$

2.3.3 Imaging System

Similar to SPIFI, in this imaging technique, optical components are used to expand and collimate the light beam before it reaches the cylindrical lens (which will provide us with the focal line). The modulation, as described in Section 2.3.2, will modulate the intensity with a chopper frequency. In Figure 9, we can visualize the assembly of the imaging technique in a summarized manner.

Figure 9 – Experimental setup of the DOIT technique. In red, we have the laser beam, which passes through the cylindrical lens (CL) generating a focal line and a Spherical Lens (SL) to focus onto the optical chopper and collimate the beam. The beam then passes through the mask and is focused by the objective lens (OL) onto the sample. Finally, the beam is focused by the Collection Optics (CO) on the detector for signal collection.

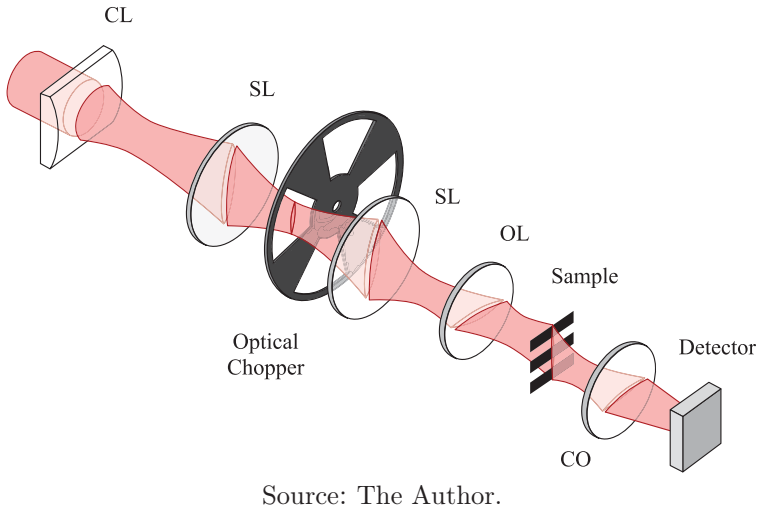

Source: The Author.

The beam is then modulated by the optical chopper in the temporal domain. As it passes through the chopper, the beam is focused onto the sample by the lens OL. This interaction can be modeled in terms of the electric field and by a function that varies in the spatial domain, as described in Section 2.3.2.

Additionally, and quite naturally, the Reflective DOIT, or ReDOIT, has also been developed. Instead of collecting the transmitted signal, the signal reflected by the sample is collected. The theory is the same as described in Section 2.3.2, and the setup can be visualized in Figure 10.

Figure 10 – Experimental setup of the ReDOIT technique. In red, we have the laser beam, which passes through the cylindrical lens (CL) generating a focal line and a Spherical Lens (SL) to focus onto the optical chopper and collimate the beam. The beam then passes through the mask and is focused by the objective lens (OL) onto the sample. Finally, the beam is focused by the Collection Optics (CO) on the detector for signal collection.

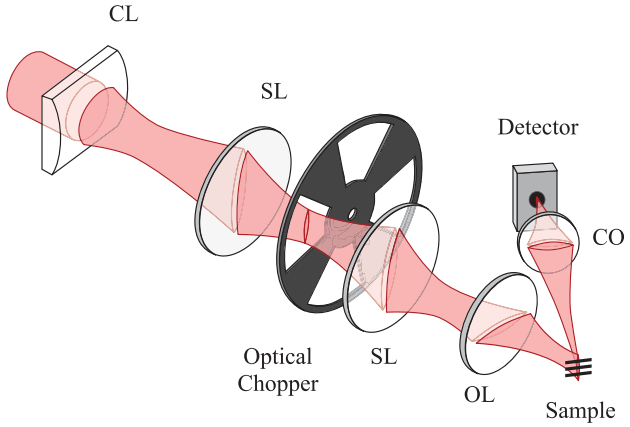

Source: The Author.

2.3.4 DOIT and ReDOIT Signal

When we modulate the intensity of the cylindrical beam and focus this beam onto a sample (or just the beam), we collect with the detector the modulation caused by the distortion due to the interaction between the beam and the object, as depicted in Figure 11.

To form a one-dimensional image, in addition to collecting the signal from the focal line along the entire sample, we must process the signal $s(t)$ by applying a temporal derivative to convert the signal into a spatial mapping, corresponding to the unique spatial locations of each point along the geometrical line, as shown in Figure 12. This temporal derivative represents a line of the magnified image.

Similar as we have high-order images in SPIFI Figure 8, in the DOIT technique, we obtain similar high-order images when applying higher-order derivatives, Figure 13 (second-order) and Figure 14 (third-order). These derivatives provide details about the

edges of the sample or how susceptible the signal is to changes related to the analyzed object.

Figure 11 – DOIT and ReDOIT Signals without a sample (black) and with a sample (needle) blocking the focal line (red). Due to the presence of the sample, part of the beam is blocked, and the collected modulation will not be the same as the pure modulation, resulting in a different signal.

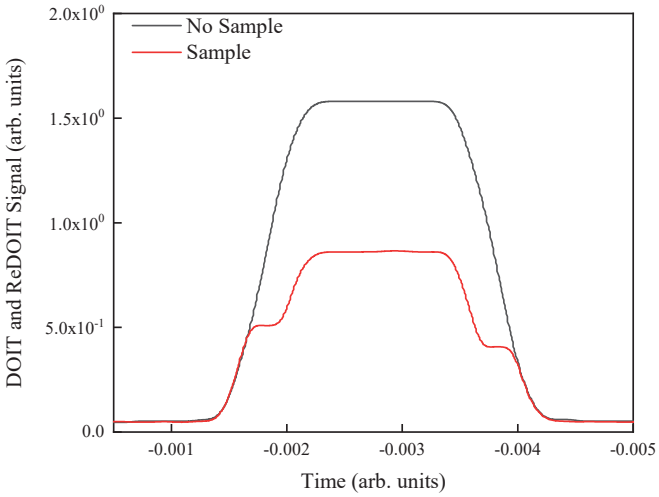

Source: The Author.

Figure 12 – DOIT and ReDOIT Derivative Signals without a sample (black) and with a sample blocking the focal line (red). It can be observed that the first-order derivative in the black signal represents a Gaussian profile modulating the beam intensity collected by the photodetector. The red signal represents the same profile, but with the sample blocking the center of the beam.

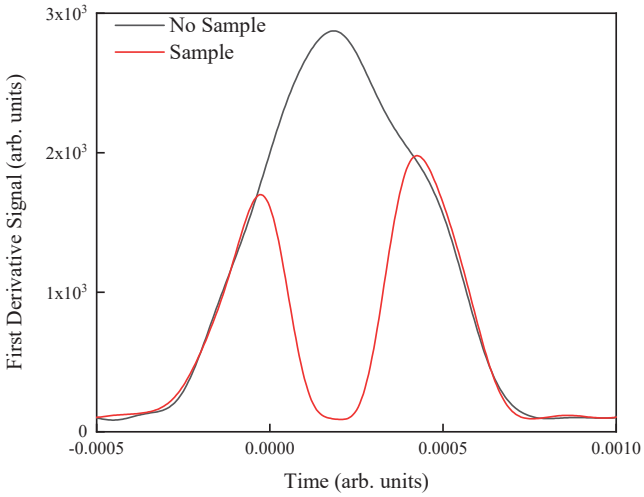

Source: The Author.

Figure 13 – DOIT and ReDOIT second-order derivative signals without a sample (black) and with a sample blocking the focal line (red). The second-order derivative indicates where transitions occur between regions of your sample.

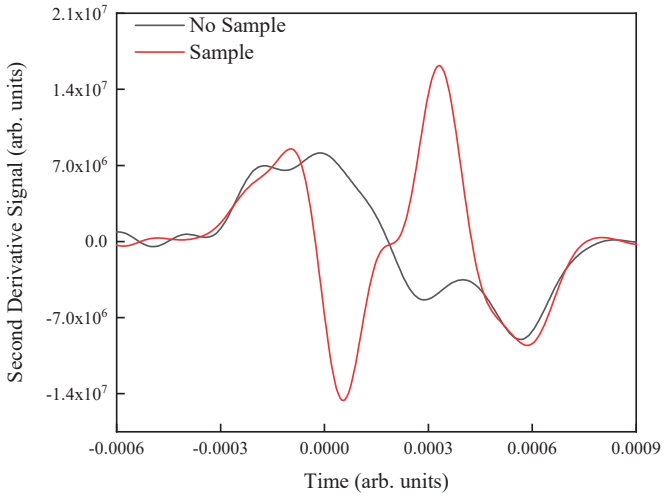

Source: The Author.

Figure 14 – DOIT and ReDOIT third-order derivative signals without a sample (black) and with a sample blocking the focal line (red). The third-order derivative indicates how quickly transitions occur between regions of your sample.

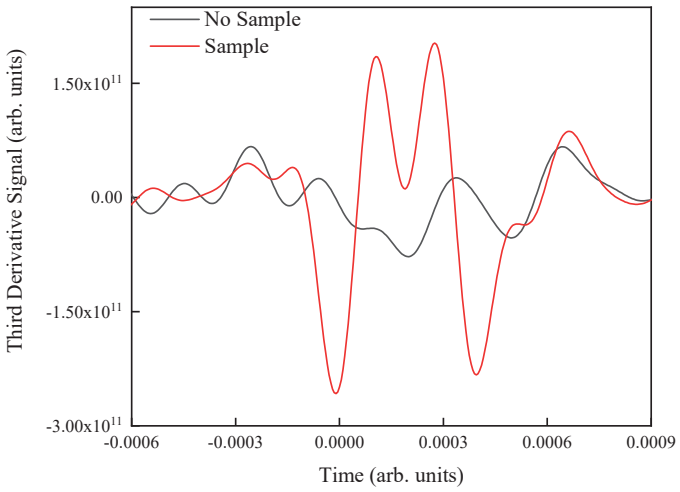

Source: The Author.

By composing images of first, second, and higher orders, it is possible to obtain a final image with enhanced sharpness and edge definition. In both techniques, SPIFI and the other method, an increase in image detail can be achieved by utilizing higher-order derivatives or harmonics. Specifically, in SPIFI, the improvement lies in the resolution, as the number of points in the image increases due to the order of the harmonic in the FFT.

— 3 —

Assembly

3.1 EXPERIMENTAL SETUP

The experimental setup of the optical imaging system can be seen in Figure 15. Note that the system is the same for the three methods implemented in this work, with only the modulation between SPIFI and DOIT/ReDOIT differing, as well as the collection method for the ReDOIT reflection signal.

Figure 15 – Experimental setup of the SPIFI, DOIT, and ReDOIT imaging systems. The difference lies solely in the modulation and whether the collected signal is the transmitted or the reflected one.

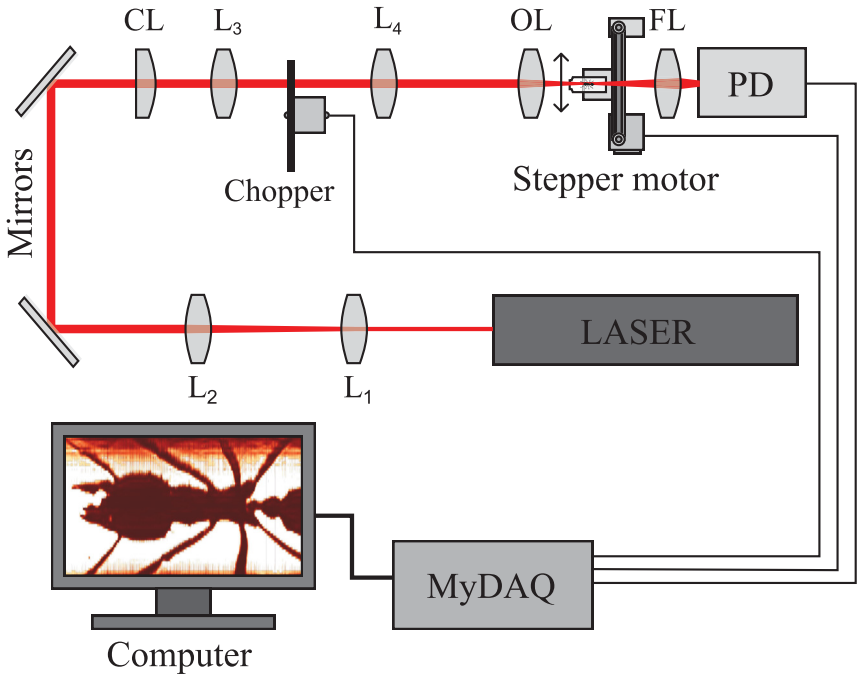

Source: Adapted from [9].

In this setup, a continuous wave (CW) *HeNe* laser (632.8 nm) with a Gaussian transverse intensity profile was used. The intensity profile varies according to a Gaussian function, as can be seen in Figures 7 and 12. Using a power meter, the laser power measured at the focus of the objective lens was 15 mW (a neutral density filter was

used to reduce the power to avoid saturating the detector). For the experiments, we used the MyDAQ device from *Emerson Electric*, which has an acquisition rate of 200 kS/s, ensuring high precision in data collection. The optical chopper, model SR540 from *Stanford Research Systems* (SRS), was operated at a frequency of 30 Hz for the DOIT and ReDOIT techniques, and at 150 Hz for the SPIFI technique.

In our setup, a neutral density filter was used to reduce the laser beam intensity by 40% to avoid saturation of the photodetector. We also employed a beam expander to collimate and expand the beam before it reaches the cylindrical lens. For this first beam expander, lenses with focal lengths of 50 mm (L_1) and 500 mm (L_2) were utilized. The second lens (L_2) was positioned at a distance that is the sum of the focal lengths, i.e., 550 mm away from the first lens (L_1).

As the light beam passes through a set of mirrors, it will go through another telescope (now in only one direction) between the cylindrical lens (CL) with a focal length of 50 mm and a spherical lens (L_3) with a focal length of 100 mm, which aims to further expand the beam and rotate it by 90 degrees so that it properly impinges on the rotating reticle. Between the focal points of lenses (L_3) and (L_4), both with a focal length of 100 mm, the modulation mask is placed to encode the cylindrical beam.

Finally, we insert the objective lens (OL), with a focal length of 30 mm, to focus the beam onto our sample. Between the lenses OL and FL, there is a sample translator that moves perpendicular to the beam propagation and the vertical extent of the focal line. The step precision between each point is 2.5 µm, which determines the resolution perpendicular to the focal line. With a focusing lens (FL) of 60 mm focal length, the signal is directed to the photodetector (PD).

3.2 SPIFI MASK

The SPIFI mask, or Lovell's reticle, is represented in Figure 16. Note that, for the cylindrical beam to be modulated, its focal line must be along the radial coordinate of the mask. Thus, when the disk is rotating, the different parts of the focal line are modulated with distinct frequencies.

3.3 DOIT/REDOIT MASK

For the DOIT and ReDOIT techniques, the modulation mask is represented in Figure 17. Note that, to modulate the cylindrical beam, it needs to be inserted perpendicular to the radial direction from the center of the chopper. Thus, when the mask is rotating, it is modulated in intensity, causing the signal to oscillate between 0 (completely blocked) and a maximum value (completely released).

Figure 16 – SPIFI mask with the cylindrical beam positioned radially to be modulated at different spatial frequencies along the radial direction.

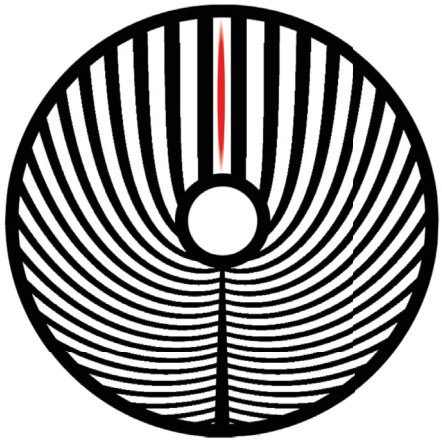

Source: The Author.

Figure 17 – Chopper mask with the cylindrical beam positioned perpendicular to the radial direction to be modulated in intensity.

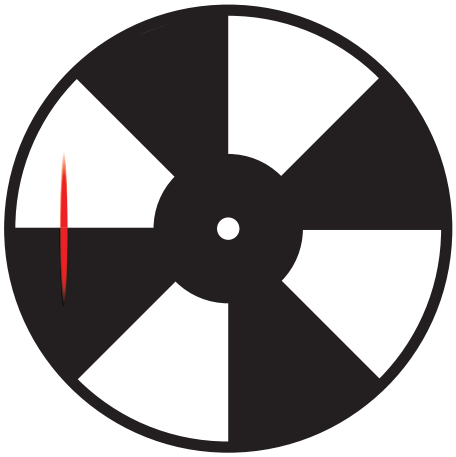

Source: The Author.

3.4 TRIPLE A PROGRAM: AUTOMATION, ACQUISITION, AND ANALYSIS

Considering the automation of the project, we developed a program using the LabVIEW programming language to move the sample in the direction perpendicular to the focal line, covering the entire sample region to obtain a two-dimensional image. Additionally, the program collects all the signals, at different positions where the sample is located, to compose the final image.

For the SPIFI technique, the dataset collected by the photodetector undergoes Fourier Transform calculation. For the DOIT and ReDOIT techniques, only the modulation signal is collected. At the end of the scan, this result is exported to a data spreadsheet for further analysis in another mathematical software.

For data analysis, a program was developed in the Mathematica software, where various types of image filters can be applied. It also allows the plotting of individual

signals for initial testing to resolution analysis.

3.5 RESOLUTION

The USAF 1951, Figure 18, resolution test is a standardized and widely used technique to assess the ability of optical systems to distinguish fine details [29, 30, 31, 32]. It utilizes a special test chart known as the United States Air Force 1951 Resolution Test Target (USAF 1951), which consists of a grid of lines and spaces arranged in specific patterns. In our setup, we used the USAF 1951 target model R3L3S1P from *Thorlabs*.

Figure 18 – Example of USAF 1951 target test. This test is used to evaluate the horizontal and vertical resolution of the imaging system.

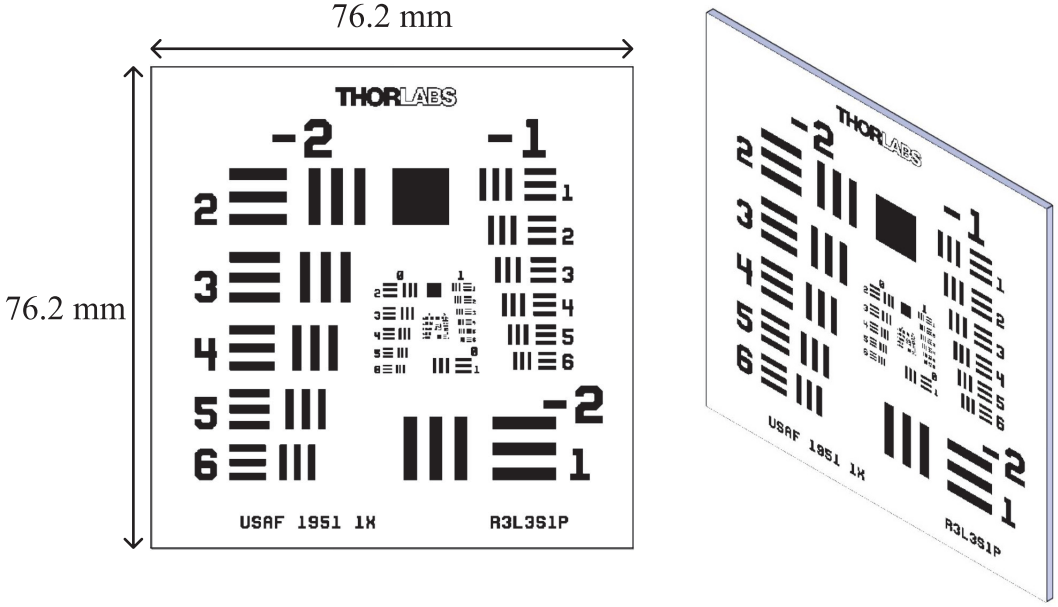

Source: A USAF 1951 R3L3S1P resolution test from *Thorlabs*.

This test chart is composed of a series of line groups, each group consisting of 6 elements. Each element contains three bars of different thicknesses and separations. The elements are provided in a standardized series of spatial frequencies given in line pairs per millimeter (lp/mm).

To perform the test, the test chart is positioned in front of the optical system under evaluation, at a focused image plane. The system captures an image of the test chart, and the smallest detail that can still be distinguished in the image is identified.

The spatial resolution of the system is then calculated based on the smallest discernible detail in the test chart image. This is usually expressed in terms of line pairs per millimeter (lp/mm). The resolution is given by:

$$\text{Resolution}\left(\frac{\text{line pair}}{mm}\right) = 2^{\,\text{Group}+\left(\frac{\text{Element}-1}{6}\right)}. \tag{3.1}$$

3.6 CONTRAST

Contrast is a fundamental aspect of image quality, dictating how effectively black and white elements can be distinguished from one another at a specified resolution [1, 2, 33]. In essence, it's about ensuring that the dark areas appear truly black and the light areas appear genuinely white. When executed correctly, this interplay between light and dark creates a well-defined image, where details emerge with clarity and precision (Figure 19).

Figure 19 – Transition from black to white is the highest contrast while intermediate greys indicate lower contrast.

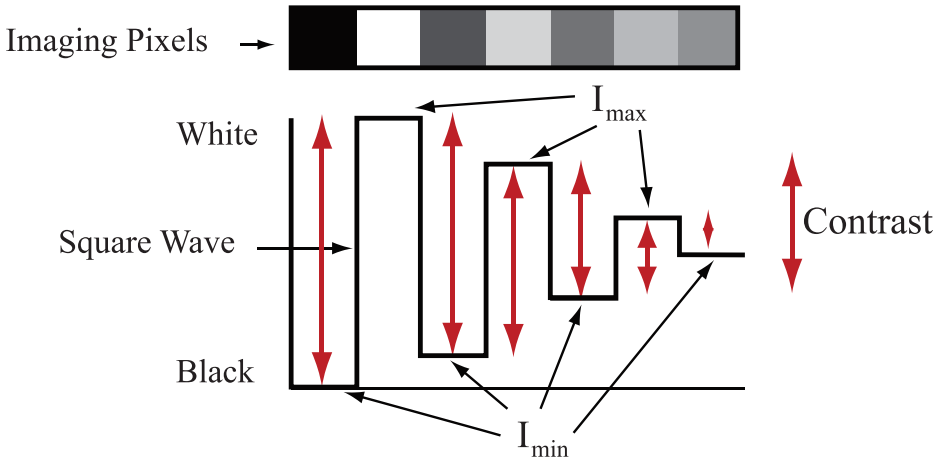

Source: The Author.

A key indicator of contrast is the extent to which black and white information remains distinct from one another, without blending into intermediate shades of grey. As black and white elements trend towards these intermediate tones, contrast at that particular frequency diminishes. Therefore, the sharper the distinction between light and dark elements, the higher the contrast. While this principle may seem self-evident, its significance cannot be understated.

Equation 3.2 provides a formal method for quantifying contrast at a given frequency. Here, I_{max} represents the maximum intensity, typically measured in pixel grayscale values, while I_{min} denotes the minimum intensity. This equation offers a quantitative means of assessing contrast, enabling precise analysis and optimization of imaging systems.

$$\% \text{ Contrast} = \left(\frac{I_{max} - I_{min}}{I_{max} + I_{min}} \right) \times 100\%. \tag{3.2}$$

3.7 SAMPLES

For initial tests on SPIFI and DOIT techniques, we used objects with simple and unique geometries, such as the one represented in Figure 5. Initially, we used a needle, Figure 20, with dimensions smaller than 1.00 mm to assess the precision and feasibility of implementing the techniques, where the modulation signals are shown in Figures 6 and 11.

Figure 20 – Magnified image of the needle obtained with a conventional optical microscope.

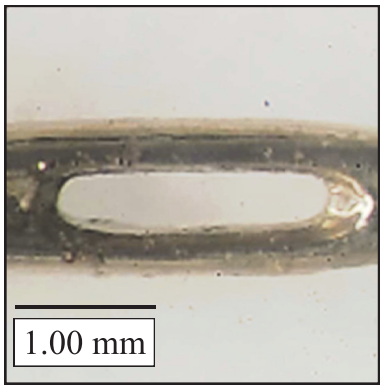

Source: The Author.

Subsequently, we used an ant of the species *Acromyrmex hispidus* (subspecies: *Acromyrmex hispidus fallax*) [34], as shown in Figure 21, commonly known as leaf-cutter ant, found mainly in urban areas in the southern region of Brazil. The leaf-cutter ant used has approximate dimensions of 6.00 mm in length and 2.00 mm in width.

Figure 21 – Magnified image of the leaf-cutter ant (*Acromyrmex hispidus fallax*) obtained with a conventional optical microscope.

Source: The Author.

As the final image, the USAF 1951 resolution test was used to demonstrate the maximum resolution obtained in the three optical imaging techniques, which can be seen in Figure 18.

— 4 —

Results

This section presents the results obtained from the stages of this research work: the automation, acquisition, and analysis program and the images obtained using the SPIFI, DOIT, and ReDOIT techniques.

4.1 AAA PROGRAM

A program was developed to handle sample movement and the collection of signals from the photodetector. For sample displacement, a stepper motor is coupled to a translation stage. Since programs developed in the LabVIEW language can be easily modified, we utilized a subroutine to drive the motor. This Sub VI, available in the article [35], can perform all motor movements, allowing for a simpler project with low cost. The files used for movement are available in the GitHub repository (https://github.com/andretec/Stepper-motor-L298-myDAQ). Sample movement and data acquisition are carried out using the myDAQ device, enabling interfacing with the computer via USB.

This program moves the sample in a direction perpendicular to the laser beam propagation axis and the extension of the focal line, sweeping across the entire sample. For the SPIFI technique, the Fourier Transform is calculated for each dataset collected by the photodetector. Conversely, for DOIT and ReDOIT, only the signal modulation is collected at each sample position. At the end of the scan, the result is exported to a data spreadsheet, allowing for the generation of a line image for each position where the laser beam was focused on the sample.

4.2 LABORATORY SETUP

The experimental setup for both techniques was successfully assembled and can be observed in Figure 15. The system posed challenges during assembly due to the sensitivity of the alignment between the lenses comprising the expanders; however, it is now aligned and fully functional for image collection via SPIFI, DOIT, and ReDOIT. The photograph in Figure 22 shows the optical table with the experimental setup for the SPIFI, DOIT, and

ReDOIT techniques. It's worth recalling that the difference between the imaging methods lies in the modulation mask employed on the chopper. SPIFI utilizes the Lovell grating, while DOIT and ReDOIT employ the traditional disk for optical choppers.

Figure 22 – Picture of SPIFI, DOIT, and ReDOIT techniques.

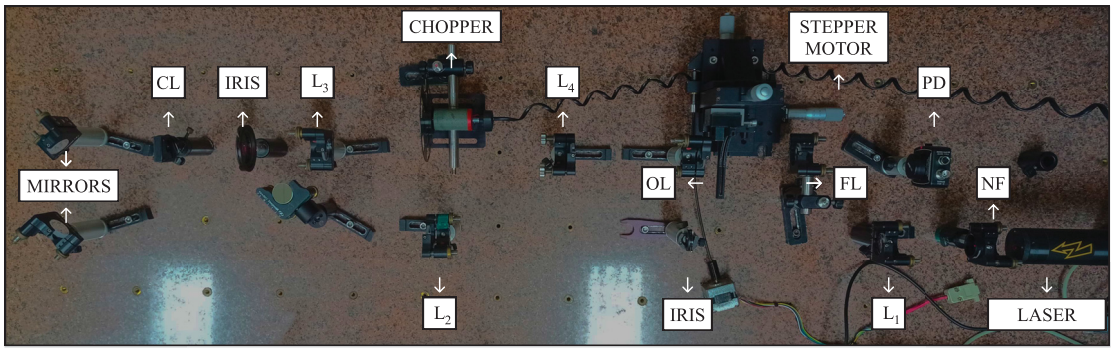

Source: The Author.

4.3 IMAGES

In this section, I will present the core of this study, featuring images of the samples to showcase the resolution achieved by the SPIFI, DOIT, and ReDOIT techniques. The images presented below feature vertical lines at specific positions to visualize the one-dimensional signal in their respective techniques. The composition of all these lines forms the two-dimensional image. For comparative purposes, the horizontal and vertical scales of all images obtained using the respective techniques are in millimeters.

4.3.1 Images by SPIFI

Figure 23 represents the first (23a) and second (23b) orders images, an enlarged image of the needle (Figure 20) obtained by the SPIFI technique:

Figure 23 – SPIFI image of the needle.

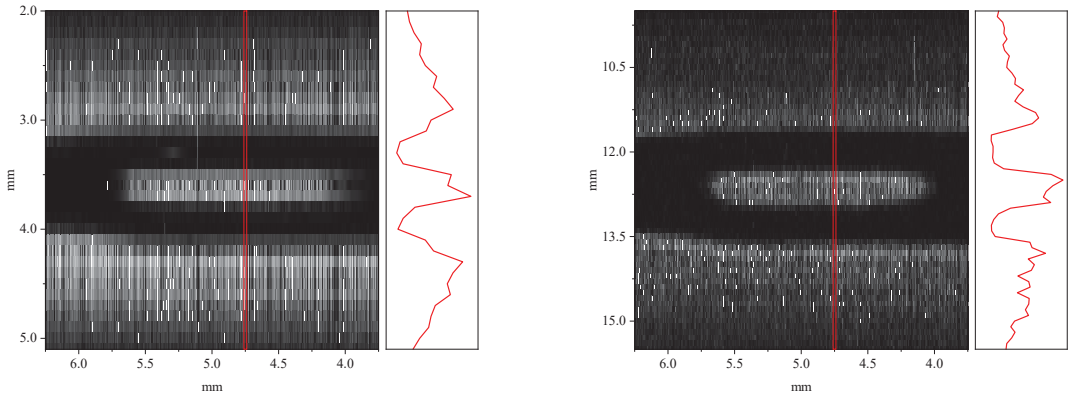

(a) First Harmonic.

(b) Second Harmonic.

Source: The Author.

Figures 24a and 24b refers to the first and second orders images of ant (Figure 21) analyzed by the SPIFI technique:

Figure 24 – SPIFI image of the ant.

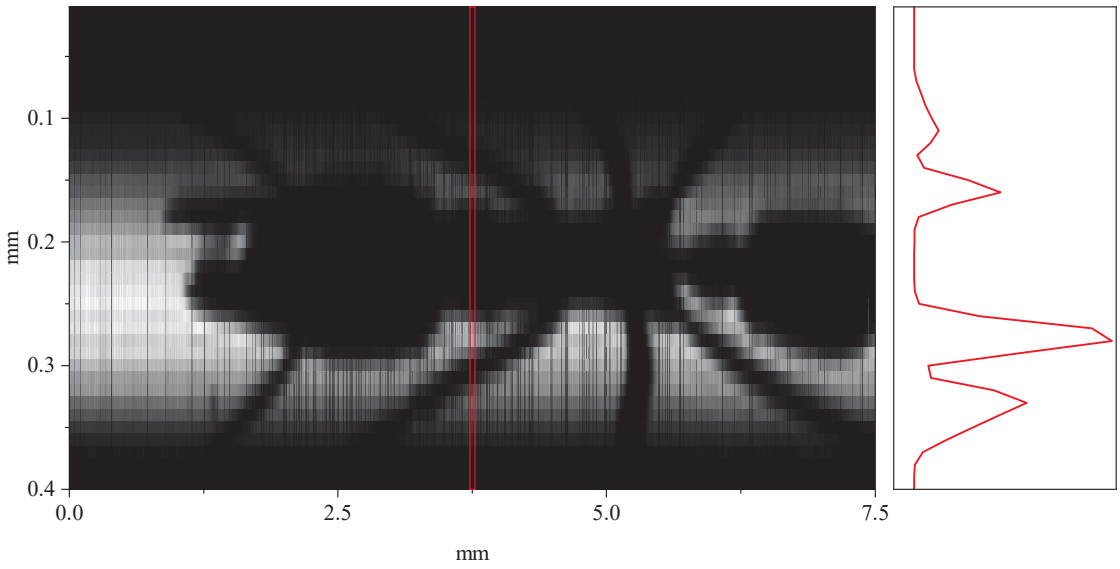

(a) First Order.

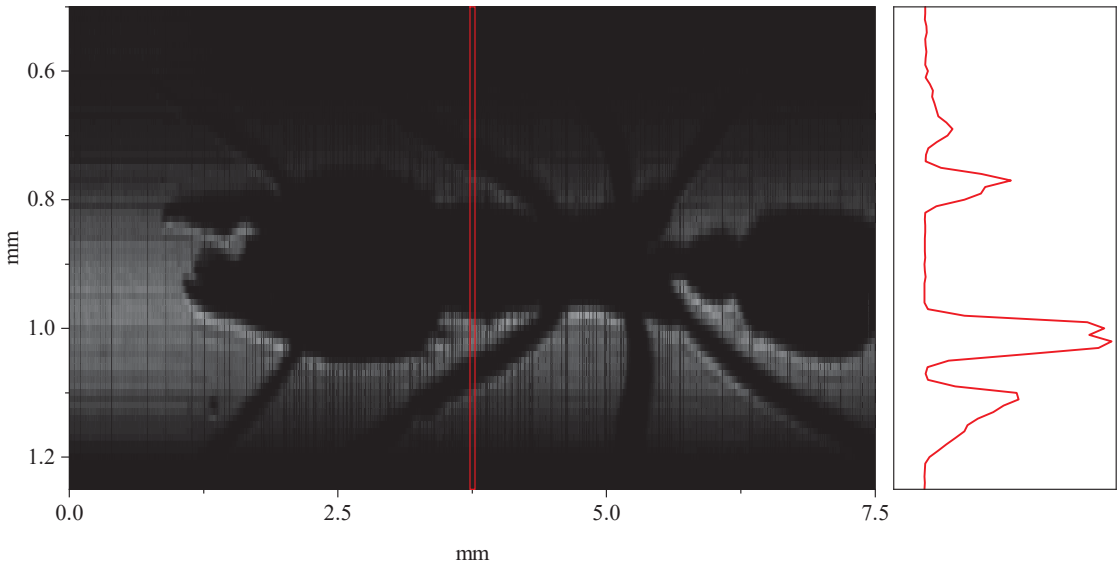

(b) Second Order.

Source: The Author.

For the USAF 1951 resolution test (Figure 18) we have Figures 25a (first order) and 25b (second order) images:

Figure 25 – SPIFI image of the Group 2 region of the 1951 USAF resolution test.

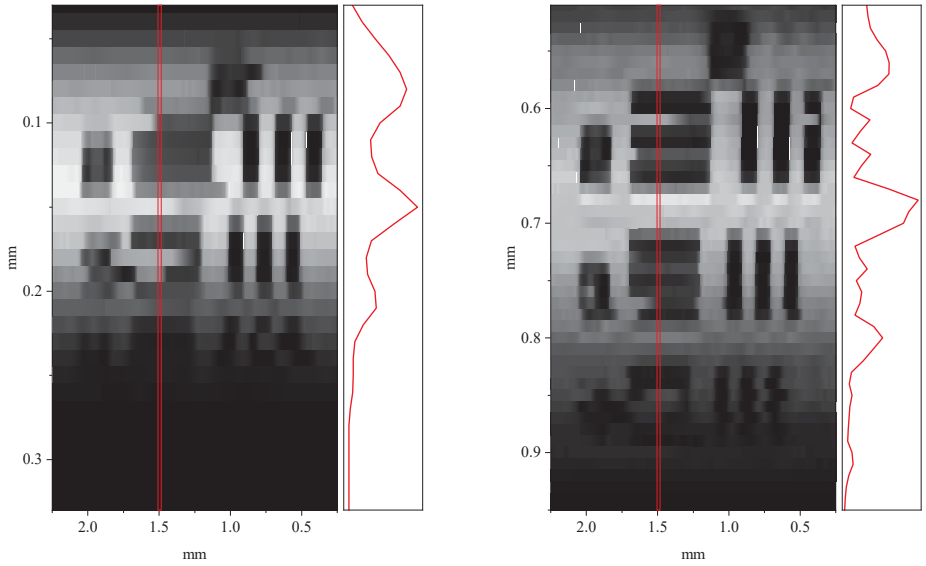

(a) First Order. (b) Second Order.

Source: The Author.

Finally, for the maximum resolution we obtain the third order image using SPIFI technique for the USAF 1951 target, represented by Figure 26:

Figure 26 – SPIFI image of the Group 2 region of the 1951 USAF resolution test.

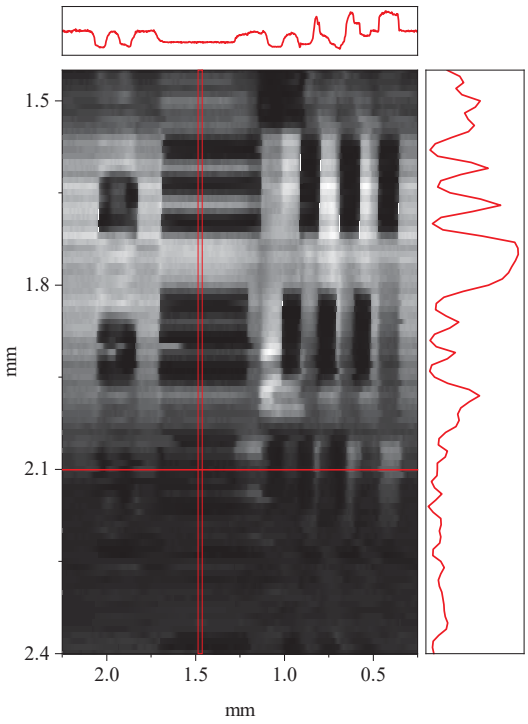

Source: The Author.

This image shows a zoomed-in view of the Group 2 region of the USAF 1951 target, used to determine the maximum resolution of the imaging system.

4.3.2 Images by DOIT

Figure 27, an enlarged image of the needle (Figure 20) obtained by the DOIT technique is visible:

Figure 27 – DOIT image of the needle.

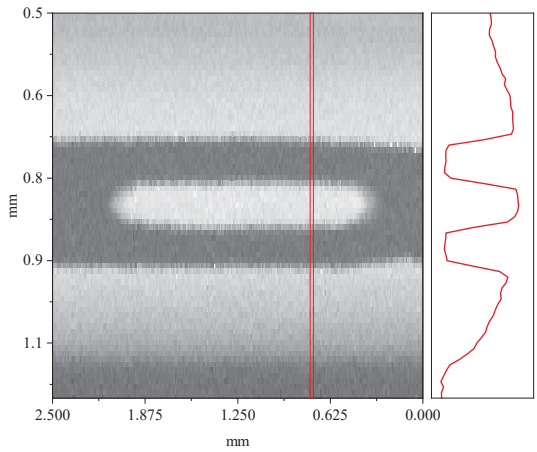

Source: The Author.

Figure 28 refers to the ant (Figure 21) analyzed:

Figure 28 – DOIT image of the ant.

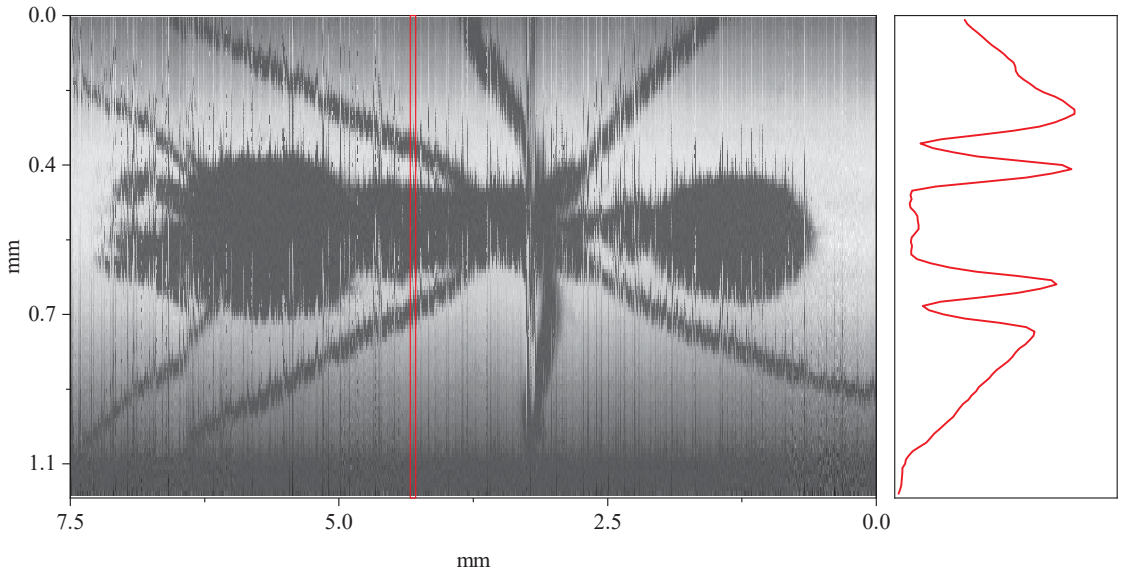

Source: The Author.

Finally, in Figure 29, we have the first (29a), second (29b), and third (29c) orders images of the USAF 1951 resolution test (Figure 18) by DOIT:

Figure 29 – DOIT image of the Group 2 region of the 1951 USAF resolution test.

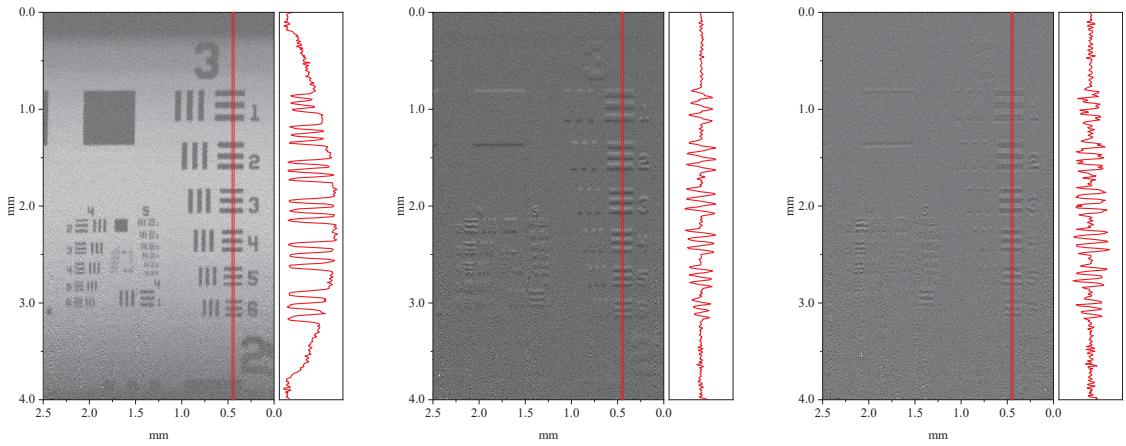

(a) First Order. (b) Second Order. (c) Third Order.

Source: The Author.

Figure 30 is the sum of the first, second, and third-order images, where we can observe a noise reduction.

Figure 30 – DOIT image of the USAF 1951 obtained by combining the three first orders.

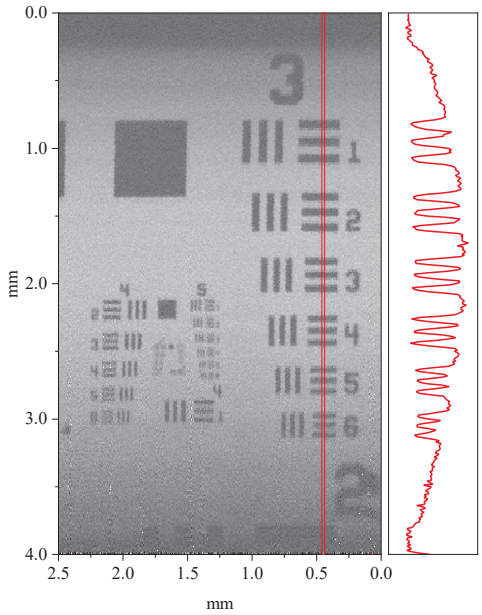

Source: The Author.

Figure 31 shows a zoomed-in view of the Group 5 region of the USAF 1951 target, used to determine the maximum resolution of the imaging system.

Figure 31 – DOIT image of the Group 5 Element 2 region of the 1951 USAF resolution test.

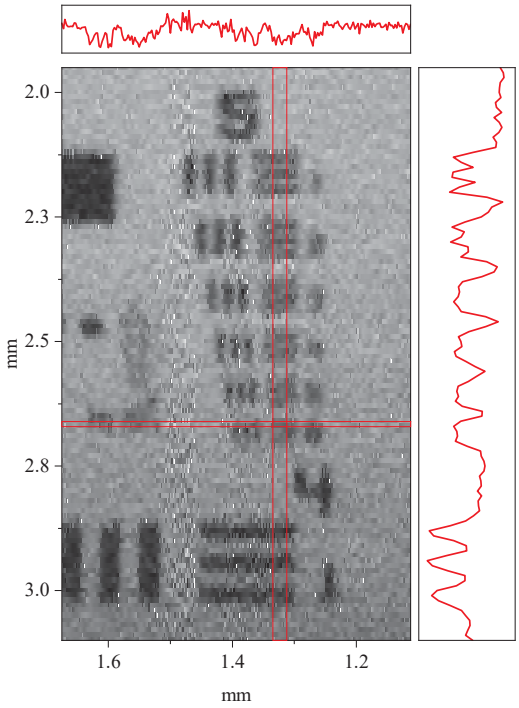

Source: The Author.

4.3.3 Images by ReDOIT

We have the final image, sum of three-order derivatives, of the USAF 1951 resolution test (Figure 18) represented in Figure 32:

Figure 32 – ReDOIT image of the Group 5 Element 2 region of the 1951 USAF resolution test.

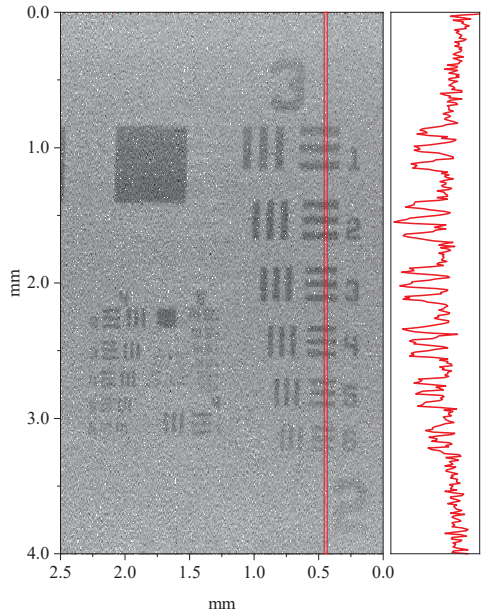

Source: The Author.

Figure 33 shows a zoomed-in view of the Group 5 region of the USAF 1951 target, used to determine the maximum resolution of the imaging system.

Figure 33 – ReDOIT image of the Group 5 region of the 1951 USAF resolution test.

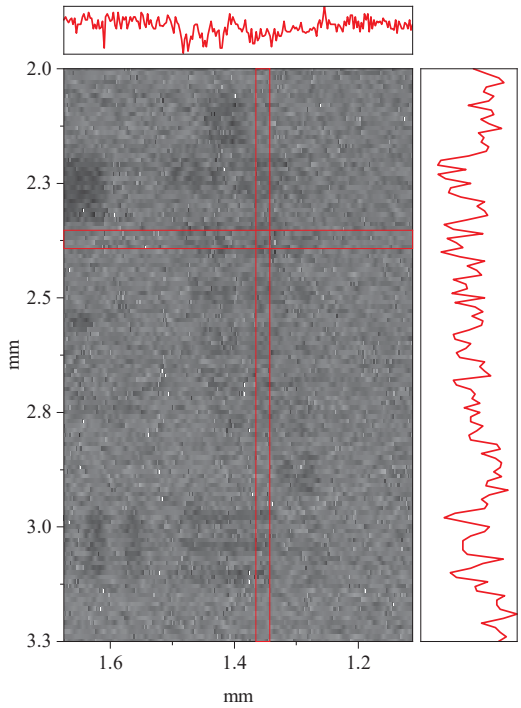

Source: The Author.

— 5 —

Discussions

Both imaging systems were successfully implemented, representing an advancement in the field of optical microscopy. An advancement of these techniques includes using a focal line for imaging and employing a single-element photodetector to collect the signal, thereby avoiding the need for CCDs and instead modulating the signal with the Lovell's reticle for SPIFI and optical chopper for DOIT and ReDOIT. Through this work, it was possible to develop imaging systems that enable efficient, fast, and cost-effective scanning imaging. Additionally, two innovative methods were introduced, which are unprecedented in the literature and promise to contribute significantly to the advancement of optical imaging techniques.

5.1 AUTOMATION

The program developed in LabVIEW proved to be a valuable tool for data analysis and project automation. In addition to performing signal acquisition and transformation, the program functions as a digital oscilloscope, allowing the analysis of complex signals such as those from SPIFI, as well as simpler signals from DOIT and ReDOIT, within specific time intervals.

To obtain a two-dimensional image of an object, position the object at the focus of the objective lens and initiate the scanning and data collection process. Although the results were demonstrated with relatively large objects to test the technique, there is the potential to improve the system's resolution by replacing the lens with a short-focus objective. This would allow for the analysis of smaller samples, enabling imaging at micrometer scales. The scanning time in our experiment is closely associated with the number of points sampled and the averaging performed at each point to reduce noise. Each point's signal is collected and averaged multiple times to ensure accuracy and minimize noise interference. As a result, our scanning procedures typically take an average of 15 minutes to form a complete image.

One challenge encountered during the project was the instability of the signal

from the photodetector, leading to overlap in the final SPIFI technique image. However, improving the SPIFI signal trigger is a possible solution to this problem, which could result in clearer images free from unwanted artifacts.

5.2 SPIFI, DOIT AND REDOIT RESOLUTION

Based on the wavelength, λ, of the laser radiation and the numerical aperture, NA, of the objective lens used, it is possible to calculate the maximum lateral resolution, d, of the microscopy system using the Rayleigh criterion $d = 0.61\lambda/(NA)$ [1, 2, 3, 31], which provides the diffraction limit. The numerical aperture (NA) is a key metric that quantifies this capability. It is defined as $\mathrm{NA} = n\lambda \cdot \sin(\theta)$ [1, 2, 3], where n represents the local refractive index, and θ denotes the maximum angle at which the imaging system collects light. This definition ties the numerical aperture directly to the system's ability to capture spatial frequencies (f_x), where f_{xmax} is the maximum spatial frequency collected. Thus, NA can also be expressed as $\mathrm{NA} = n \cdot f_{\mathrm{xmax}}$. For the microscope in question, a one-inch diameter lens (25.4 mm) with a focal length of 30 mm was used, so that $NA \approx 0.3898$. Considering $\lambda = 632.8\,\mathrm{nm}$, we have $d \approx 990\,\mathrm{nm}$. Therefore, we can say that 990 nm is the theoretical limit for the lateral resolution of the optical microscope used, assuming it is perfectly aligned and that the entire numerical aperture of the objective lens is being utilized.

In the case of the SPIFI microscope, where the focal line is modulated along its length, there are different resolutions in the direction of the focal line and perpendicular to it. The thickness of the focal line provides the resolution in the direction perpendicular to the line (horizontal axis in Figures 23 and 24), which in our experiment is $\approx 2.4\,\mu$m, given that we are illuminating only around 40% of the diameter of the objective lens, LO. Since the smallest sample step in the direction perpendicular to the focal line is 2.5 µm, this defines our resolution in this direction. However, experimentally, this factor is limited by the thickness of the beam focused on the sample. If the beam thickness is smaller than the step size, then indeed the translational step becomes the limiting factor.

Along the focal line (vertical axis in Figures 23 and 24), the resolution can be found by dividing the length of the line projected on the sample, ≈ 3.4 mm, by the number of distinct frequencies produced by the modulation. For this case, we have a total of 30 distinct frequencies for the first order (Figures 23a and 24a), which led to a resolution of approximately $113\,\mu$m. For the second-order image (Figures 23b and 24b) the focal line was encoded with 60 different frequencies, representing a resolution of approximately $57\,\mu$m. Note that the second-order signal has twice the frequencies compared to the first-order signal, which is theoretically expected. As can be seen, the more frequencies used to divide the focal line, the better the resolution of the system in this direction, bearing in mind that in both directions, the resolution can only be optimized up to the diffraction

limit of the system, which is 990 nm.

In the latest measurements with the USAF 1951 target for the SPIFI technique, the resolution obtained was lower than that found in previous results, as reported in our earlier publication [9]. The reason for this discrepancy is primarily related to the timing of data acquisition and the focus on developing and refining the DOIT and ReDOIT techniques. As a result, the system was not optimized for the SPIFI technique during these measurements. Note that in the first and second-order images for the SPIFI technique, it is not possible to clearly distinguish the vertical and horizontal lines, as shown in Figures 25a and 25b. However, as we increase the number of pixels in the image by analyzing the third-order image, it becomes possible to distinguish the test bars. The resolution observed, as shown in Figure 26, was approximately 198 μm, corresponding to group 2 element 3 for the third-order image. For SPIFI contrast, we have 97.1% for the first-order image (Figure 25a), 96.7% for the second-order image (Figure 25b), and 96.3% for the third-order image (Figure 26). Note that the contrast obtained in the first, second, and third-order images remained consistent. This stability suggests that the modulation performed by the SPIFI technique effectively maintained the ratio between maximum and minimum intensities across different image orders. Constant contrast values indicate the technique's ability to preserve signal quality and signal-to-noise ratio at various spatial frequencies. This reduced resolution highlights the need for proper system optimization to achieve the best possible results with the SPIFI technique. However, it is worth mentioning that it has already been shown that it is possible to obtain super-resolution images, i.e., with resolution below the diffraction limit, when nonlinear optical processes are employed using the SPIFI technique [6].

Observing Figure 26 some artifacts can be seen cutting the image vertically. These dark lines are present due to the difficulty of performing the *trigger* of the SPIFI signal in the LabVIEW software, due to the complexity of this signal. Thus, when the signal oscillates, the position of the SPIFI signal is lost, and then the transform of a noise is calculated, generating a line with values inconsistent with the real image. This problem can be solved by using more stable reference channels or by monitoring how the signal changes along the sample to better control the trigger.

The spatial resolution and the ability to distinguish between closely spaced points in an image are crucial characteristics for any imaging system. While many systems rely on multiple spatial frequencies to achieve this resolution, our technique utilizes only a single spatial frequency determined by the chopper. Nevertheless, the ability to distinguish between closely spaced points, essential for spatial resolution, is maintained. This is achieved through the temporal modulation of the excitation beam, which allows for capturing detailed information about the sample even with a single spatial frequency.

In the case of DOIT, where the focal line is modulated along its length, distinct

resolutions are achieved in the direction of the focal line (y) and perpendicular to it (x). Since the smallest step of the sample in the direction perpendicular to the focal line is 2.5 μm, this becomes our limiting factor and thus our resolution in this direction. However, analyzing Figure 31, the limiting resolution in the x direction corresponds to group 6, element 1 of the USAF-1951 Test Target, which reaches 15.6 μm. Analyzing Figure 33, the resolution found in the horizontal direction corresponds to group 5, element 2, achieving achieving 27.9 μm for ReDOIT. This discrepancy, compared to the precision of the translator, may be due to the optical system, specifically the width of the focal line defined by the objective lens. Additionally, the signal from the closest lines may not be visible due to its magnitude being below the noise level. Additionally, the difference in resolution between the axes could cause some information from the x-axis to be lost in the noise of the y-axis. As we can see in Figures 31 and 33, the limiting resolution in the direction of the focal line (y) of the optical system used corresponds to group 5, element 2 of the USAF-1951 test target. This is equivalent to 35.9 line pairs per millimeter, or 27.9 μm, with a contrast of 66.1%, for DOIT, and 33.3%, for ReDOIT. In electromagnetic optics [2], it is fundamental that the sum of the transmission (T), reflection (R), and absorption (A) coefficients equals 1. This relationship can be verified through the contrast signal in both techniques.

It's worth noting that this resolution can be enhanced by replacing the objective lens with one that has a higher numerical aperture (NA). A higher NA lens can capture finer spatial details by collecting light from a wider range of angles, allowing the system to resolve higher spatial frequencies f_{xmax}. Additionally, lenses with shorter focal lengths can improve the sharpness of smaller features within the sample. Upgrading to a lens with a higher NA and possibly a shorter focal length would improve the overall resolution of our optical imaging setup.

In our current setup, we utilize the MyDAQ data acquisition system with a sampling rate of 200 kSamples/second and the SR540 optical chopper operating at frequencies of 30 Hz for DOIT and ReDOIT techniques. This setup allows us to collect data points at a rate of 400 points per half modulation cycle. Given that the beam size at the focus of the objective lens is approximately 3.4 mm, we have a spatial distribution of 400 points over this 3.4 mm line.

The density of points in our current configuration is calculated by dividing the number of points by the beam size, resulting in approximately 117.65 points per millimeter. To enhance the resolution of our imaging system, it is crucial to increase the number of points collected per modulation cycle while maintaining the same acquisition rate and beam size.

One effective way to achieve this is by reducing the frequency of the optical chopper. Lowering the chopper frequency increases the time available for each modulation

cycle, allowing more data points to be collected within the same spatial interval. Thus, by reducing the chopper frequency, we can increase the number of points per half modulation cycle. This increase in point density enhances the resolution of our imaging system, allowing for more detailed spatial analysis of the sample. By optimizing the frequency of the optical chopper, we can achieve higher resolution imaging without altering the existing acquisition rate or beam size.

Identifying the temporal axis as the encoded y coordinate and the x-axis as the translation axis, the image is successfully obtained from either halves of the signal, corresponding to the incoming and outgoing of the blade across the sample, and the sample is identified on points with temporal derivative ds/dt near zero, as predicted, and without the need for smoothing. The spatial distribution of the object can often be inferred without derivation. With a fixed width and height of the image, we also managed to make a contrast between the normalized images of a sample and the pure modulation. If the system parameters are kept the same for different images, the same data can be used to remove the modulation.

For comparative purposes of higher orders between Fourier Transform harmonics and derivatives, the SPIFI technique achieves a gain in resolution (the number of points in the image), while the gain in the DOIT derivatives is in image sharpness (edge enhancement).

— 6 —

Conclusions

In conclusion, this study successfully implemented and explored novel optical imaging techniques: SPIFI, DOIT, and ReDOIT. These techniques represent significant advancements in the field of optical microscopy, offering efficient and cost-effective for scanning imaging. One notable feature is their utilization of a focal line for scanning the sample. By modulating this focal line, the signal can be collected using a single-element photodetector, thus eliminating the need for a CCD camera. The experimental setup utilized state-of-the-art equipment, including the MyDAQ data acquisition system and the SR540 optical chopper, which operated at frequencies of 30 Hz for DOIT and ReDOIT and 150 Hz for SPIFI.

Automation through LabVIEW played a crucial role in improving data acquisition and analysis by automating system control for scanning and signal collection. This software facilitated precise control over experimental parameters and data processing for SPIFI, DOIT, and ReDOIT techniques. Future enhancements could include integrating a controller on the translational stage, parallel to the beam propagation axis, to automate sample positioning at the objective focus, further enhancing experimental efficiency and accuracy.

Resolution analysis revealed distinct capabilities between the techniques. SPIFI demonstrated potential for high-resolution imaging through spatial frequency modulation, while DOIT and ReDOIT utilized temporal modulation to enhance image sharpness and edge detection. Looking ahead, future improvements could focus on refining the optical setup to maximize numerical aperture and minimize noise interference. Enhancing these aspects could significantly improve the spatial and temporal resolution of the imaging systems, making them essential tools for applications in biomedical research, materials science, and other advanced fields.

In summary, this work contributes to the ongoing advancement of optical imaging techniques, highlighting their versatility and potential for advancing scientific understanding and technological innovation.

— 7 —

Future

The DOIT and ReDOIT techniques developed and analyzed throughout this thesis show significant potential for a variety of future applications across different scientific and technological fields.

Employing low modulation frequencies [36], there is the potential to capture a broader temporal window in the collected signal. This extended temporal window enables the observation of signal variations over longer time scales within the sample. Thus, low modulation in DOIT or ReDOIT may be advantageous where the dynamics of the sample evolve slowly or exhibit long-duration phenomena. For the resolution perpendicular to the line, it is directly related to the optics of the system and the precision of the translation stage used. In other words, the minimum resolution is the one that has displacement steps on the order of diffraction. It is important to note that there should be a minimum frequency limit where the signal contrast becomes lower than the noise. Due to the limitations of the MyDAQ data acquisition device, there is a cap on the number of data points obtained per second (maximum sampling rate is 200 kS/s), which prevents sufficient data acquisition at very low frequencies.

A promising application of the DOIT and ReDOIT techniques lies in the early detection of melanoma, an aggressive type of skin cancer [37]. The ability of these techniques to identify subtle changes at the edges of samples is crucial for diagnosing melanoma, which often features irregular border variations. Utilizing DOIT/ReDOIT can significantly improve the accuracy and speed of diagnoses, aiding physicians and dermatologists in making more informed clinical decisions. Additionally, these techniques can be extended to other medical fields, such as tissue analysis in biopsies, where edge detection and structural variations are essential.

Extending the DOIT and ReDOIT techniques to the Terahertz (THz) region opens new opportunities in fields such as material inspection, security, and quality control. The THz region is known for its unique properties, including the ability to penetrate various non-conductive materials like plastics, ceramics, and fabrics, and provide high contrast in images. This makes THz imaging particularly useful for identifying internal

defects, contaminations, or inclusions in industrial products, such as manufacturing flaws in electronics or structural weaknesses in composites.

One of the significant challenges in THz imaging is the lack of suitable cameras capable of capturing images at these wavelengths. Traditional imaging systems are inadequate due to the unique optical properties of THz radiation. This is where the Single-Pixel Imaging (SPI) technique becomes highly advantageous. By using a single-pixel detector and computational reconstruction methods, SPI can overcome the limitations posed by the absence of THz cameras. The DOIT and ReDOIT techniques, when adapted for SPI in the THz range, can offer a robust solution for high-resolution imaging without relying on expensive and complex multi-pixel detectors.

In security applications, THz imaging can be utilized to detect concealed objects and substances, such as explosives or drugs, through clothing and packaging, providing a non-invasive and safe inspection method. In the pharmaceutical industry, THz spectroscopy combined with imaging can analyze the composition and quality of pharmaceutical products, ensuring consistency and safety in drug manufacturing.

Using light sources in the Extreme Ultraviolet (XUV) region, with wavelengths around 40 nm, can significantly enhance resolution. This spectral range allows for the visualization of nanoscale details, which is particularly useful in nanosciences and materials engineering. Applying DOIT and ReDOIT techniques in this region can revolutionize material characterization, enabling the observation of nanometric structures with unprecedented precision. This advancement has direct implications in fields such as semiconductor manufacturing, where detailed inspection of surfaces and interfaces is crucial.

The resolution of images obtained with DOIT and ReDOIT techniques can be further enhanced by optimizing the system's optical components. Currently, we use an objective lens with a 30 mm focus; however, replacing it with short-focus objective lenses can considerably increase resolution. By focusing the laser beam into a shorter focal line, we can improve the spatial resolution capability of the techniques, allowing the capture of finer and more precise details. This adjustment is particularly beneficial for applications in metrology and surface analysis, where precision is paramount.

The DOIT and ReDOIT techniques demonstrate extraordinary potential to expand the horizons of optical imaging in various fields. Melanoma detection, applications in Terahertz and Extreme Ultraviolet regions, and optical optimization for higher resolution are just a few of the many possibilities that can be explored in the future. These advancements will not only enhance the accuracy and applicability of optical imaging techniques but also open new pathways for research and development in diverse areas, from medicine to materials science and industrial security.

References

[1] BORN, M.; WOLF, E. **Principles of Optics: Electromagnetic Theory of Propagation, Interference and Diffraction of Light**. [S.l.]: Cambridge University Press, 1999. Cit. on pp. 12, 33, 44.

[2] HECHT, E. **Optics**. [S.l.]: Addison-Wesley, 2016. Cit. on pp. 12, 33, 44, 46.

[3] GOODMAN, J. W. **Introduction to Fourier Optics**. [S.l.]: McGraw-Hill Series in Electrical and Computer Engineering, 2011. Cit. on pp. 12, 44.

[4] SHEETZ, K. E.; HOOVER, E. E.; CARRILES, R.; KLEINFELD, D.; SQUIER, J. A. **Advancing multifocal nonlinear microscopy: development and application of a novel multibeam Yb:KGd (WO4) 2 oscillator**. Optics express, Optica Publishing Group, v. 16, n. 23, p. 17574–17584, 2008. Cit. on pp. 12, 16.

[5] GORA, M.; KARNOWSKI, K.; SZKULMOWSKI, M.; KALUZNY, B. J.; HUBER, R.; KOWALCZYK, A.; WOJTKOWSKI, M. **Ultra high-speed swept source OCT imaging of the anterior segment of human eye at 200 kHz with adjustable imaging range**. Optics express, Optica Publishing Group, v. 17, n. 17, p. 14880–14894, 2009. Cit. on pp. 12, 15.

[6] FIELD, J. J.; WERNSING, K. A.; DOMINGUE, S. R.; ALLENDE MOTZ, A. M.; DELUCA, K. F.; LEV, D. H.; DELUCA, J. G.; YOUN, M. D.; SQUIER, J. A.; BARTELS, R. A. **Superresolved multiphoton microscopy with spatial frequency-modulated imaging**. Proceedings of the National Academy of Sciences, National Acad Sciences, v. 113, n. 24, p. 6605–6610, 2016. Cit. on pp. 12, 16, 45.

[7] YOUNG, M. D.; BARBANO, E. C.; WORTS, N.; FIELD, J. J.; HOY, C.; WERNSING, K. A.; BARTELS, R. A.; SQUIER, J. **Spatial Frequency Modulated Imaging (SPIFI) with Amplitude or Phase Grating from a Spatial Light**

Modulator. Sensors and Actuators A: Physical, Elsevier, v. 233, p. 509–515, 2015. Cit. on pp. 12, 16.

[8] WORTS, N.; CZERSKI, J.; JONES, J.; FIELD, J. J.; BARTELS, R.; SQUIER, J. **Simultaneous multi-dimensional spatial frequency modulation imaging**. International Journal of Optomechatronics, Taylor & Francis, v. 14, n. 1, p. 1–17, 2020. Cit. on pp. 12, 16.

[9] SOARES, Y. S.; MACHADO, M. J.; MISOGUTI, L.; BARBANO, E. C. **Imageamento Óptico com Fotodetector de Elemento Único**. Revista Brasileira de Ensino de Física, Sociedade Brasileira de Física, v. 39, n. 4, e4401, 2023. Cit. on pp. 12, 17, 18, 21, 29, 45.

[10] LI, X.; LI, J.; LI, Y.; OZCAN, A.; JARRAHI, M. **High-throughput terahertz imaging: progress and challenges**. Light: Science & Applications, Nature Publishing Group, v. 12, p. 233, 2023. Cit. on p. 12.

[11] FANG, J.; HUANG, K.; WU, E.; YAN, M.; ZENG, H. **Mid-infrared single-photon 3D imaging**. Light: Science & Applications, Nature Publishing Group, v. 12, p. 144, 2023. Cit. on p. 12.

[12] KILCULLEN, P.; OZAKI, T.; LIANG, J. **Compressed ultrahigh-speed single-pixel imaging by swept aggregate patterns**. Light: Science & Applications, Nature Publishing Group, v. 12, p. 144, 2023. Cit. on p. 12.

[13] FUTIA, G.; SCHLUP, P.; WINTERS, D. G.; BARTELS, R. A. **Spatially-chirped modulation imaging of absorbtion and fluorescent objects on single-element optical detector**. Optics Express, v. 19, n. 2, p. 1626–1640, 2011. DOI: 10.1364/OE.19.001626. Available from: https://www.osapublishing.org/oe/abstract.cfm?uri=oe-19-2-1626. Cit. on pp. 13, 17–20, 23.

[14] MARVIN, M. **Microscopy apparatus**. 1961. US3013467A. Cit. on p. 15.

[15] THIMSEN, E.; SADTLER, B.; BEREZIN, M. Y. **Shortwave-infrared (SWIR) emitters for biological imaging: a review of challenges and opportunities**. Nanophotonics, v. 6, n. 5, p. 1043–1054, 2017. DOI: doi:10.1515/nanoph-2017-0039. Available from: https://doi.org/10.1515/nanoph-2017-0039. Cit. on p. 15.

[16] RADWELL, N.; MITCHELL, K. J.; GIBSON, G. M.; EDGAR, M. P.; BOWMAN, R.; PADGETT, M. J. **Single-pixel infrared and visible microscope**. Optica, Optica Publishing Group, v. 1, n. 5, p. 285–289, 2014. DOI: 10.1364/OPTICA.1.000285. Available from: https://opg.optica.org/optica/abstract.cfm?URI=optica-1-5-285. Cit. on p. 15.

[17] DHAR, N. K.; DAT, R.; SOOD, A. K. **Advances in Infrared Detector Array Technology**. In: Rijeka: Optoelectronics, IntechOpen, 2013. chap. 7. DOI: 10.5772/51665. Available from: https://doi.org/10.5772/51665. Cit. on p. 15.

[18] EDGAR, M.; GIBSON, G.; BOWMAN, R.; AL., et. **Simultaneous real-time visible and infrared video with single-pixel detectors**. Sci Rep, Nature Publishing Group, v. 5, p. 10669, 2015. DOI: 10.1038/srep10669. Available from: https://doi.org/10.1038/srep10669. Cit. on p. 15.

[19] GIBSON, G. M.; SUN, B.; EDGAR, M. P.; PHILLIPS, D. B.; HEMPLER, N.; MAKER, G. T.; MALCOLM, G. P. A.; PADGETT, M. J. **Real-time imaging of methane gas leaks using a single-pixel camera**. Opt. Express, Optica Publishing Group, v. 25, n. 4, p. 2998–3005, 2017. DOI: 10.1364/OE.25.002998. Available from: https://opg.optica.org/oe/abstract.cfm?URI=oe-25-4-2998. Cit. on p. 15.

[20] DAVIDOVITS, P.; EGGER, M. D. **Scanning Laser Microscope**. **Nature**, Springer Science and Business Media LLC, v. 223, n. 5208, p. 831–831, 1969. DOI: 10.1038/223831a0. Available from: https://doi.org/10.1038/223831a0. Cit. on p. 16.

[21] SHEPPARD, C.; CHOUDHURY, A. **Image Formation in the Scanning Microscope**. Optica Acta: International Journal of Optics, Informa UK Limited, v. 24, n. 10, p. 1051–1073, 1977. DOI: 10.1080/713819421. Available from: https://doi.org/10.1080/713819421. Cit. on p. 16.

[22] SCHAWLOW, A. L.; TOWNES, C. H. **Infrared and Optical Masers**. Phys. Rev., American Physical Society, v. 112, p. 1940–1949, 6 1958. DOI: 10.1103/PhysRev.112.1940. Available from: https://link.aps.org/doi/10.1103/PhysRev.112.1940. Cit. on p. 16.

[23] HOOVER, E. E.; YOUNG, M. D.; CHANDLER, E. V.; LUO, A.; FIELD, J. J.; SHEETZ, K. E.; SYLVESTER, A. W.; SQUIER, J. A. **Remote focusing for programmable multi-layer differential multiphoton microscopy**. Biomed. Opt.

Express, v. 2, n. 1, p. 113–122, 2011. DOI: 10.1364/BOE.2.000113. Available from: http://www.osapublishing.org/boe/abstract.cfm?URI=boe-2-1-113. Cit. on p. 16.

[24] SANDERS, J. S.; DRIGGERS, R. G.; HALFORD, C. E.; GRIFFIN, S. T. **Imaging with frequency-modulated reticles**. **Optical Engineering**, v. 30, p. 1720–1724, 1991. Available from: https://api.semanticscholar.org/CorpusID:121371651. Cit. on pp. 17, 18, 23.

[25] MOTZ, A. M. A.; CZERSKI, J.; ADAMS, D. E.; DURFEE, C.; BARTELS, R.; FIELD, J.; HOY, C. L.; SQUIER, J. **Two-dimensional random access multiphoton spatial frequency modulated imaging**. Optics Express, v. 28, n. 1, p. 405–424, 2020. DOI: 10.1364/OE.378460. Available from: https://www.osapublishing.org/oe/fulltext.cfm?uri=oe-28-1-405&id=425565. Cit. on p. 18.

[26] BLOCK, E.; YOUNG, M. D.; WINTERS, D. G.; FIELD, J. J.; BARTELS, R. A.; SQUIER, J. A. **Simultaneous spatial frequency modulation imaging and micromachining with a femtosecond laser**. Optics Letters, v. 41, n. 2, p. 265–268, 2016. DOI: 10.1364/OL.41.000265. Available from: https://www.osapublishing.org/ol/abstract.cfm?uri=ol-41-2-265. Cit. on p. 18.

[27] SKOGEN, B. J. **Numerical Modeling and Ray Tracing of Spatial Frequency Modulation For Imaging**. Thesis (PhD in Physics) – Colorado School of Mines (CSM), EUA, Golden, 2018. Available from: https://mountainscholar.org/handle/11124/172820. Cit. on p. 18.

[28] LOVELL, D. J. **Electro-optic position indicator system**. 1959. US2997699A. Cit. on p. 18.

[29] KANG, D.; YOO, H.; JILLELLA, P.; BOUMA, B. E.; TEARNEY, G. J. **Comprehensive volumetric confocal microscopy with adaptive focusing**. Biomed. Opt. Express, Optica Publishing Group, v. 2, n. 6, p. 1412–1422, 2011. DOI: 10.1364/BOE.2.001412. Available from: https://opg.optica.org/boe/abstract.cfm?URI=boe-2-6-1412. Cit. on p. 32.

[30] SÁNCHEZ-ORTIGA, E.; SHEPPARD, C. J. R.; SAAVEDRA, G.; MARTÍNEZ-CORRAL, M.; DOBLAS, A.; CALATAYUD, A. **Subtractive imaging in confocal scanning microscopy using a CCD camera as a detector**. Opt. Lett., Optica Publishing Group, v. 37, n. 7, p. 1280–1282, 2012. DOI:

10.1364/OL.37.001280. Available from:
https://opg.optica.org/ol/abstract.cfm?URI=ol-37-7-1280. Cit. on p. 32.

[31] YOUNG, M. D. **Developments in Multifocal Multiphoton Microscopy with Single Element Detection**. Thesis (PhD in Physics) – Colorado School of Mines (CSM), EUA, Golden, 2015. Available from:
https://mountainscholar.org/handle/11124/17114. Cit. on pp. 32, 44.

[32] YUAN, H.; ZHANG, X.; WANG, F.; WANG, W.; XU, M. **Resolution enhancement for flexible microscopic imaging based on dictionary learning**. Opt. Express, Optica Publishing Group, v. 28, n. 23, p. 35047–35060, 2020. DOI: 10.1364/OE.403317. Available from:
https://opg.optica.org/oe/abstract.cfm?URI=oe-28-23-35047. Cit. on p. 32.

[33] SIEGMAN, A. E. **Lasers**. [S.l.]: University Science Books, 1986. Cit. on p. 33.

[34] CAMPOS, A. E.; BUENO, O.; MORINI, M. **Formigas em Ambientes Urbanos no Brasil**. 1. ed. [S.l.]: Canal 6, 2017. P. 685. ISBN 978-85-7917-456-8. Cit. on p. 34.

[35] ROMERO, A. L. S.; BARBANO, E. C.; MISOGUTI, L. **Sistema computadorizado para deslocamento de amostra com motor de passo utilizando o L298: aplicação na técnica de varredura-Z**. Rev. Bras. Ensino Fís., v. 41, n. 4, e20190018-1 - e20190018–9, 2019. DOI: 10.1590/1806-9126-RBEF-2019-0018. Available from:
https://doi.org/10.1590/1806-9126-rbef-2019-0018. Cit. on p. 35.

[36] MACHADO, M. J.; SZUSZKO, Y. S.; CIONEK, M. P.; MISOGUTI, L.; BARBANO, E. C. **Laser Scanning Microscope Utilizing Modulated Signal Derivatives: Studies on Resolution and Higher-Order Differentiation**. 2024 Autumn Meeting of the Brazilian Physical Society, 2024. Available from:
https://sec.sbfisica.org.br/eventos/eosbf/2024/programa/pesqAutor.asp. Cit. on p. 49.

[37] HEATON, A. R.; BURKARD, N. J.; SONDEL, P. M.; SKALA, M. C. **Quantifying in vivo collagen reorganization during immunotherapy in murine melanoma with second harmonic generation imaging**. Biophoton. Discovery, v. 1, n. 1, p. 015004, 2024. Available from: https://doi.org/10.1117/1.BIOS.1.1.015004. Cit. on p. 49.